Folded Well-Defined 3D Architecture from Synthetic Helical and Sheet-Like Polymers

*Chengyuan Wang, Arielle Mann, Regina H. Garvey, Bianca L. Dumlao, Matthew D. Hannigan, and Marcus Weck**

Department of Chemistry and Molecular Design Institute, New York University, 100 Washington Square East, New York, NY 10003
E-mail: mw125@nyu.edu

Keywords: poly(isocyanide), poly(*p*-phenylene vinylene), [2.2]paracyclophane-1,9-diene, secondary structures, single-chain polymeric nanoparticles (SCNP)

Abstract

The fabrication of truly hierarchically folded single-chain polymeric nanoparticles with primary, secondary, and defined three-dimensional (3D) architecture, is still an unfulfilled goal. In this contribution, we report a polymer that folds into a well-defined 3D structure from a synthetic sheet-helix block copolymer. The sheet-like poly(*p*-phenylene vinylene) (PPV) block is synthesized via the ring-opening metathesis polymerization of a thymine-bearing dialkoxy-substituted [2.2]paracyclophane-1,9-diene. The PPV was terminated with a Pd catalyst via a Pd-containing chain-terminating agent. The terminal Pd complex catalyzes the polymerization of isocyanide monomers with side-chains containing either a chiral menthol or a diaminopyridine resulting in the formation of a helical poly(isocyanide) (PIC) random copolymer. The PIC side-chains are capable of undergoing three hydrogen bonds with the complementary thymine units along the PPV block resulting in the folding of the two secondary structural domains into a well-defined 3D structure. The folding and unfolding of the polymer in both chloroform and THF were monitored using dynamic light scattering and NMR spectroscopy. This work is the first example of a hierarchically folded synthetic polymer featuring a defined 3D structure achieved by using two different polymer backbones with two distinct secondary structures.

1. Introduction

Proteins' hierarchical structures are composed of amino acid sequences that fold into secondary and tertiary structures.[1-2] The folding events among peptidic domains occur between precisely arranged motifs using noncovalent interactions such as hydrogen bonding, Coulombic interactions, and hydrophobic interactions, as well as dynamic covalent bonds.[3] This structural diversity endows proteins with function. Unstable protein conformations and structures under non-native environments, however, limit the applications of these natural polymers. Synthetic polymers have the advantage of tunable stability, backbone diversity, and easy scalability. Creating protein mimetic structures using fully synthetic polymers, therefore, can promote the development of polymer structure-property relationships and generate advanced materials for catalysis,[4-12] imaging,[13-17] and drug delivery.[17-21]

True hierarchical structures that mimic proteins require primary, secondary, and tertiary structures incorporated into the same molecule.[1] In synthetic polymer chemistry, strategies towards this goal can be categorized into two categories: single-chain polymeric nanoparticles (SCNPs)[4, 22-24] and main-chain block copolymers.[25-26] The SCNP strategy imitates the folding process using intramolecular interactions. Different covalent chemistries, such as copper-catalyzed alkyne-azide cycloaddition,[27] thiol-ene click chemistry,[28] photodimerization,[29-30] disulfide bond,[31] Michael addition,[10] Diels-Alder reaction,[32] and noncovalent interactions, such as hydrogen bonding,[33-39] hydrophobic interactions,[9, 40] host-guest chemistry,[38, 41-42] and metal coordination,[11, 43] are used to fold specific regions within a single polymer chain to generate a collapsed particle with a defined 3D conformation. The main-chain block copolymer approach, on the other hand, focuses on the incorporation of each block featuring a distinct secondary structure to mimic proteins. This method uses synthetic polymers with defined secondary structures connected covalently or noncovalently to generate protein-like structures.[25] Complex protein structures require both, secondary structural elements and precisely controlled intramolecular interactions, to drive folding processes, i.e. this natural process combines the advantages of both strategies.

While various helical polymers and helical assemblies have been reported in protein-mimetic polymers,[9, 26, 35, 37, 44] the incorporation of sheet-mimicking components is limited.[26, 37, 45-46] Current methods towards fully synthetic polymers containing both helical and sheet-like structures have been reported by the Meijer group and us.[9, 26, 35, 37, 45-47] Functionalizing the

polymers' side-chains with benzene-1,3,5-tricarboxamides, a hydrogen bonding mediated self-assembly building block, the Meijer group introduced a helical domain within folded SCNPs.[9, 35, 37] They included hydrogen-bonded ureido-pyrimidinone dimers to form sheet-like domains in the SCNPs.[37] Our group, instead, focuses on helical polymers such as poly(isocyanide)s (PIC) and poly(methacrylamide)s and the sheet-like polymer poly(*p*-phenylene vinylene) (PPV) to mimic different peptides' secondary structures. Combining these secondary structure-bearing synthetic polymers, we have synthesized linear assemblies of multiple secondary structures.[26, 45-47] In particular, we have reported a covalent sheet-helix block copolymer system that incorporates sheet-like PPV and helical PIC polymers using a chain-extension strategy.[45-46] A bifunctional reagent with a vinyl ether moiety and an alkyne-Pd complex was synthesized to terminate the ring-opening metathesis polymerization (ROMP) of [2.2]paracyclophane-1,9-diene (pCpd) resulting in the terminal installment of a Pd complex that catalyzes the polymerization of phenyl isocyanides.[45] A sheet-helix block copolymer was prepared that exhibited the fluorescence property of the PPV block and the helical features of the PIC block.[45] We further demonstrated the synthesis of sheet-coil-helix and coil-sheet-helix covalent block copolymers using poly(norbornene) as a coil-mimetic domain.[46]

To pursue the fabrication of structurally similar proteins using synthetic polymers with carbon-based backbones, we rationalize that a single block copolymer system containing molecular recognition groups along the side-chains of secondary structure-bearing polymers to drive folding is critical. While we have reported the side-chain functionalization of helical PIC with various supramolecular recognition units,[48-51] PPVs synthesized via ROMP with side-chain functionalities, however, are absent from the literature.[52] Recently, our group developed a method to append functional side-chains to pCpd for their incorporation into PPV by a living polymerization. Using boron tribromide, aryl ether side-chains can be selectively cleaved to generate pCpds with a hydroxy moiety that can be substituted with functional side-chains using a facial substitution reaction.[53] In this contribution, we report the combination of our CTA strategy that can terminate the ROMP of functionalized pCpds with the polymerization of functional phenyl isocyanides,[45] to generate sheet-helix block copolymers with complementary hydrogen bonding pairs along the side-chains (**Figure 1**). Using thymines (Thy) along the PPV side-chains and diaminopyridines (DAP) attached to the PIC side-chains, the sheet-helix block copolymer folds into a well-defined 3D structure with two distinct secondary domains via hydrogen bonding. The

prepared block copolymer and its folding behavior are characterized by ^{1}H NMR spectroscopy, diffusion-ordered spectroscopy (DOSY), circular dichroism (CD), UV and fluorescence spectroscopies, and dynamic light scattering (DLS).

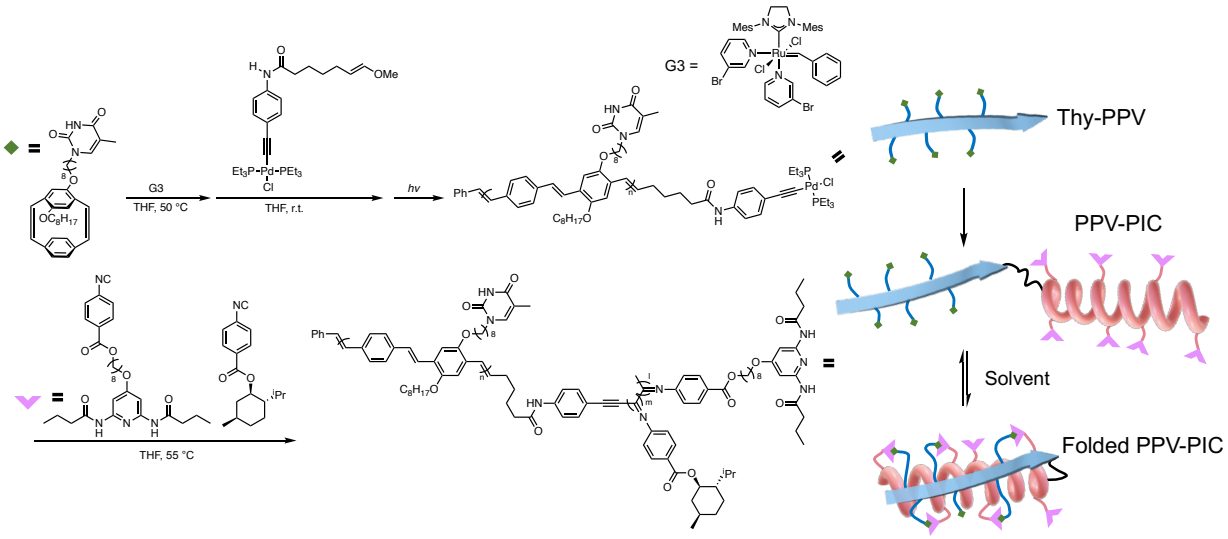

Figure 1. Schematic representation of the preparation of the sheet-helix block copolymers and their folding into defined-3D architecture mediated by hydrogen bonding interactions.

2. Results and Discussion

2.1. Synthesis and characterization of DAP-PIC

To enable the complementary hydrogen bonding association between different blocks, the block copolymer design requires functional isocyanide monomers with DAP units and pCpd monomers with Thy units. The DAP-containing isocyanide (DAP-PhNC (**3**)) was designed to include an octyl linker between the phenyl isocyanide and the DAP to provide good solubility and to decouple the DAP from the polymer backbone (**Scheme 1**). The esterification of 8-bromooctanol and phenyl formamide carboxylic acid with 4-dimethylaminopyridine and 1-ethyl-3-(3-dimethylaminopropyl)carbodiimide afforded the bromo terminated phenyl formamide. The terminal bromide was substituted with DAP to generate the formamide precursor which was dehydrated using phosphoryl chloride and triethylamine to generate the DAP-bearing phenyl isocyanide monomer **3**. To obtain PICs with a preferred handedness, a *L*-menthol-based phenyl isocyanide (*L*-Men-PhNC) was prepared according to literature procedures and was used as the comonomer to induce the helical conformation of the polymer backbone.[54] We targeted a degree

of polymerization (DP) of 100 with 10 eq. of DAP-PhNC and 90 eq. of *L*-Men-PhNC. We rationalized that, because of the rigid rod-like shape of the PIC chain, the DAP units must be dispersed randomly along the backbone to increase the probability of hydrogen bonding between the DAP units and the complementary Thy units attached to the PPV block. Copolymerization kinetic experiments of the two monomers using an alkyne-Pd catalyst were carried out using a total monomer concentration of 0.1 M and [M]:[I] = 100 (**Figure 2**). The polymerization progress was monitored using gel-permeation chromatography (GPC) and the conversion vs time plot (Figure 2b) shows that the two monomers polymerize at the same rate suggesting that a copolymer of these two monomers will be random with the DAP side-chains randomly dispersed along the backbone. The copolymer (**DAP-PIC**) composed of 90 *L*-Men-PhNC and 10 DAP-PhNC repeat units was obtained (M_n = 22.8 kDa, $Đ$ = 1.14) and the characteristic protons of the DAP and menthol groups were observed in the ^{1}H NMR spectrum (Figure 2c).

Next, we investigated the hydrogen bonding capability of the helical copolymer, which is critical for driving the folding of the block polymer. Upon addition of one eq. of *N*-hexylthymine, the amide proton signal of the DAP groups along the copolymer side-chains shifted downfield to 9.12 ppm (Figure 2d). The amide proton signal shifted to 9.80 ppm after the addition of three eq. of *N*-hexylthymine. The association constant of the DAP with the *N*-hexylthymine groups was calculated to be 947 ± 58 M^{-1} in $CDCl_3$ at room temperature as determined by ^{1}H NMR titration experiments by following the chemical shifts of DAP amide protons. This value is comparable to reported polymeric examples of the DAP-Thy association constant indicating that the association ability of DAP connected to the PIC backbone is not affected by the backbone.[55-57]

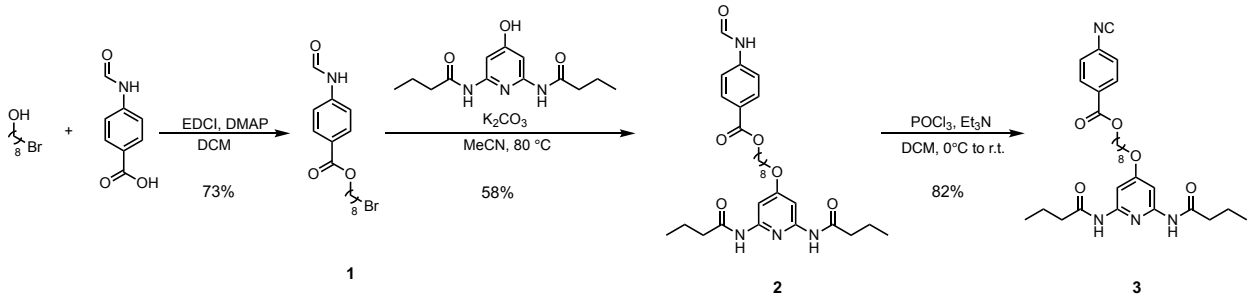

Scheme 1. Synthetic route towards DAP-PhNC.

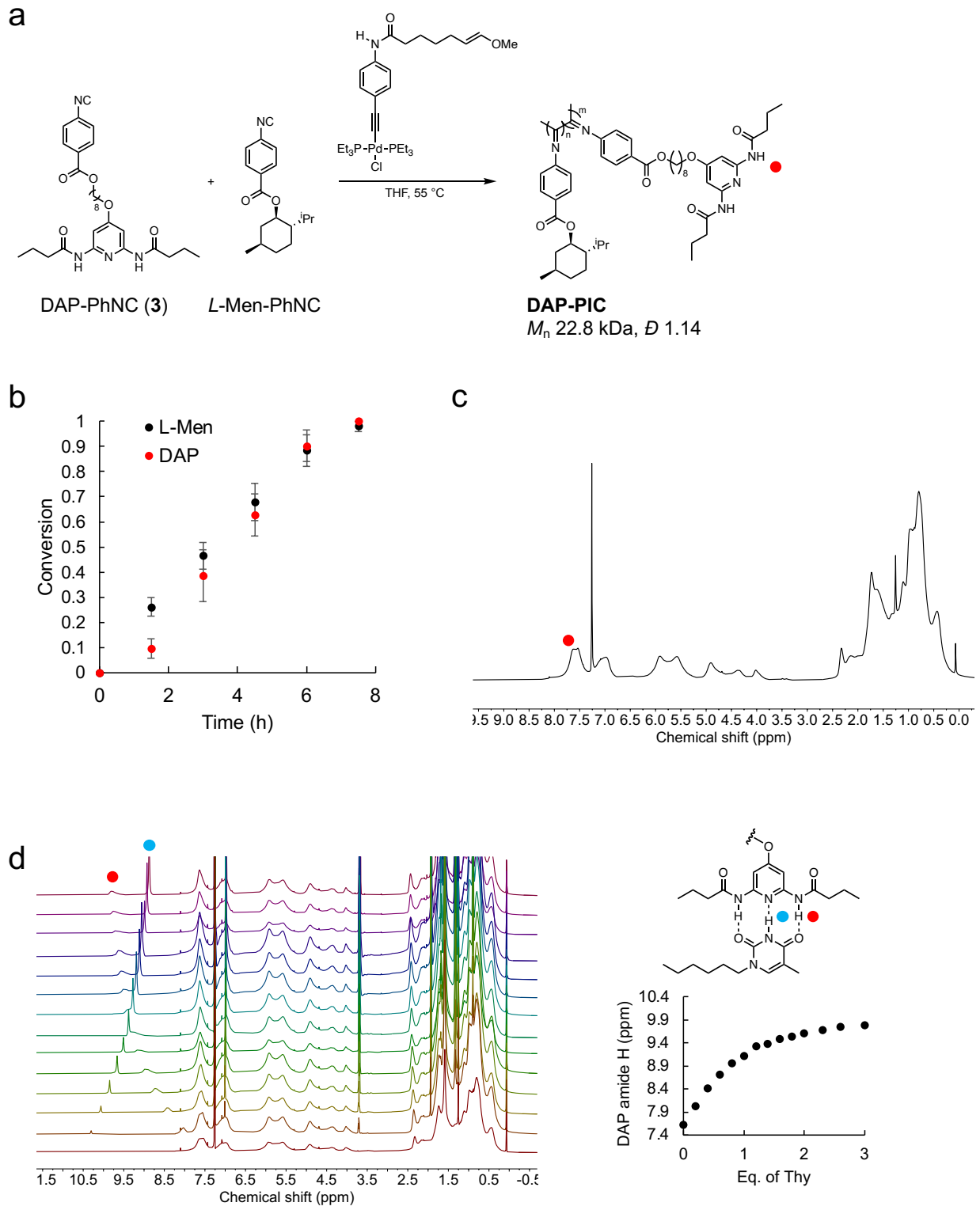

Figure 2. a) Schematic representation of the copolymerization of DAP-PhNC and *L*-Men-PhNC. b) Polymerization kinetics of the DAP-PhNC and *L*-Men-PhNC at a concentration of 0.1 M in THF. c) ^{1}H NMR spectrum of **DAP-PIC** in $CDCl_3$. d) ^{1}H NMR titration spectra and the chemical shifts

of *N*-hexylthymine to **DAP-PIC** by following the signal of the DAP amide protons in $CDCl_3$ at 0.005 M (based on repeat units).

As a copolymer of chiral and achiral monomers, **DAP-PIC** was confirmed to be a helical polymer by a positive Cotton effect at around 360 nm, indicating a right handedness of the helical backbone (**Figure 3**a). The CD spectra recorded in THF and chloroform have the same pattern but differ slightly in the intensity and position of the maxima: In THF, the maximum peak lies at 358 nm while it shifts to 362 nm in chloroform (Figure 3a). Interestingly, the UV-Vis absorption spectra (Figure 3b) of **DAP-PIC** in THF and chloroform also differ as a shoulder is visible around 310 nm in the spectrum in chloroform while the intensity of the peak at 250 nm decreases compared to the spectrum in THF. We hypothesize that these observations originate from small differences of the arrangement of the phenyl groups connected to the PIC backbone as a result of the difference of solvent polarities between the two solvents.[58] Nonetheless, the helicity of the polymer backbone is untouched by switching the solvents.

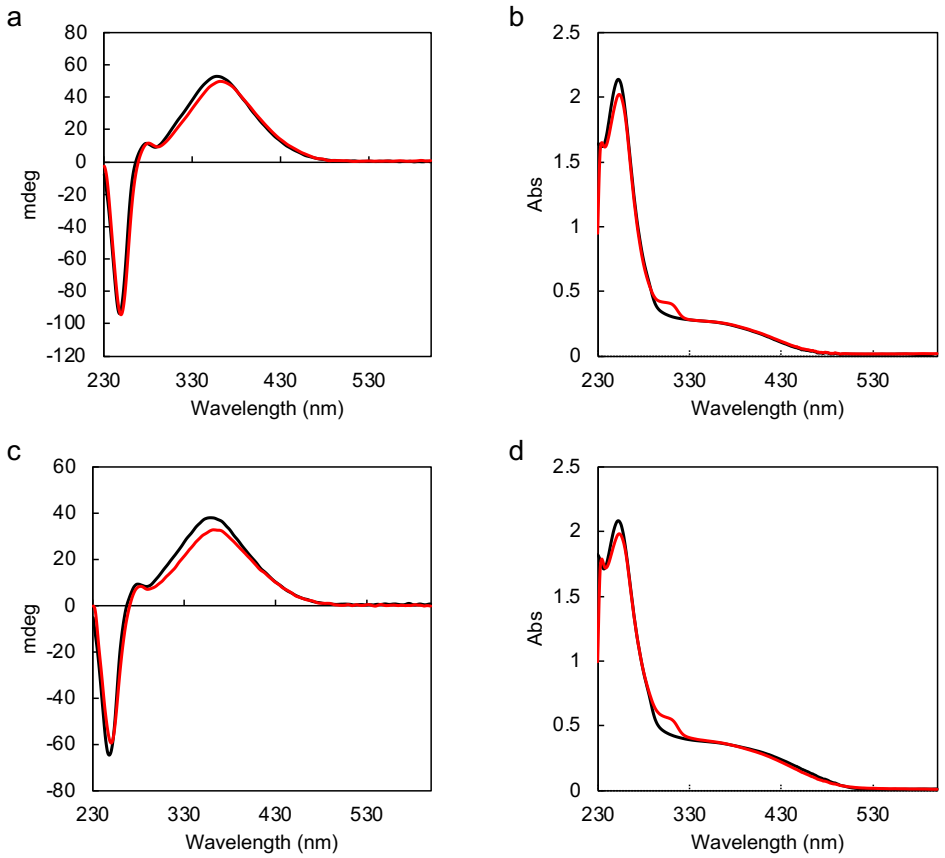

Figure 3. CD and UV-Vis spectra of (a, b) **DAP-PIC** and (c, d) **PPV-PIC** in THF (black) and chloroform (red) at 0.2 mg mL^{-1}.

2.2 Synthesis and characterization of Thy-PPV

The dioctyloxy-pCpd was prepared according to literature procedures.[26] One octyl side-chain was selectively cleaved from the pCpd using three equivalents of BBr_3 to generate a pCpd with one octyloxy side-chain and one phenol group. An octylbromide side-chain was connected to the phenolic OH group of the pCpd using 1,8-dibromooctane under basic conditions. The side-chain was further substituted with the Thy unit through the substitution of the terminal bromide group using cesium carbonate to yield the target Thy-pCpd monomer (**6**) (**Scheme 2a**).

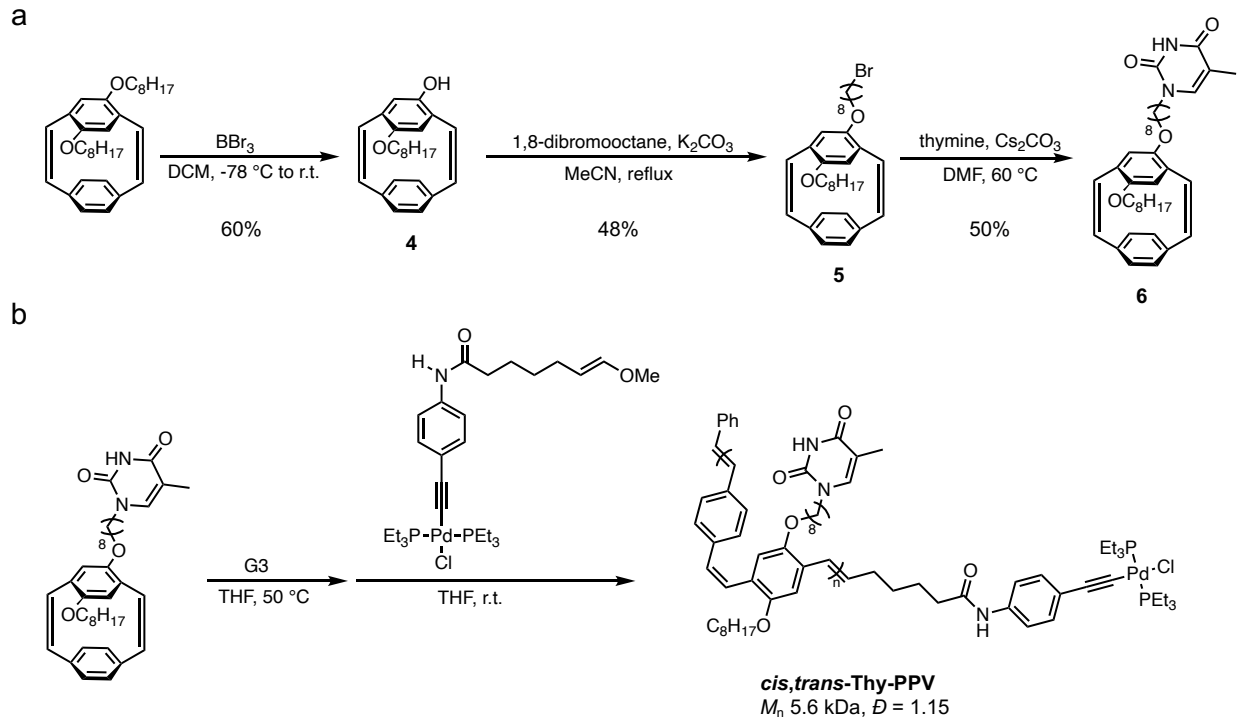

Scheme 2. a) Synthetic route towards Thy-pCpd. b) Schematic representation of the polymerization of Thy-pCpd using Grubbs' third generation initiator.

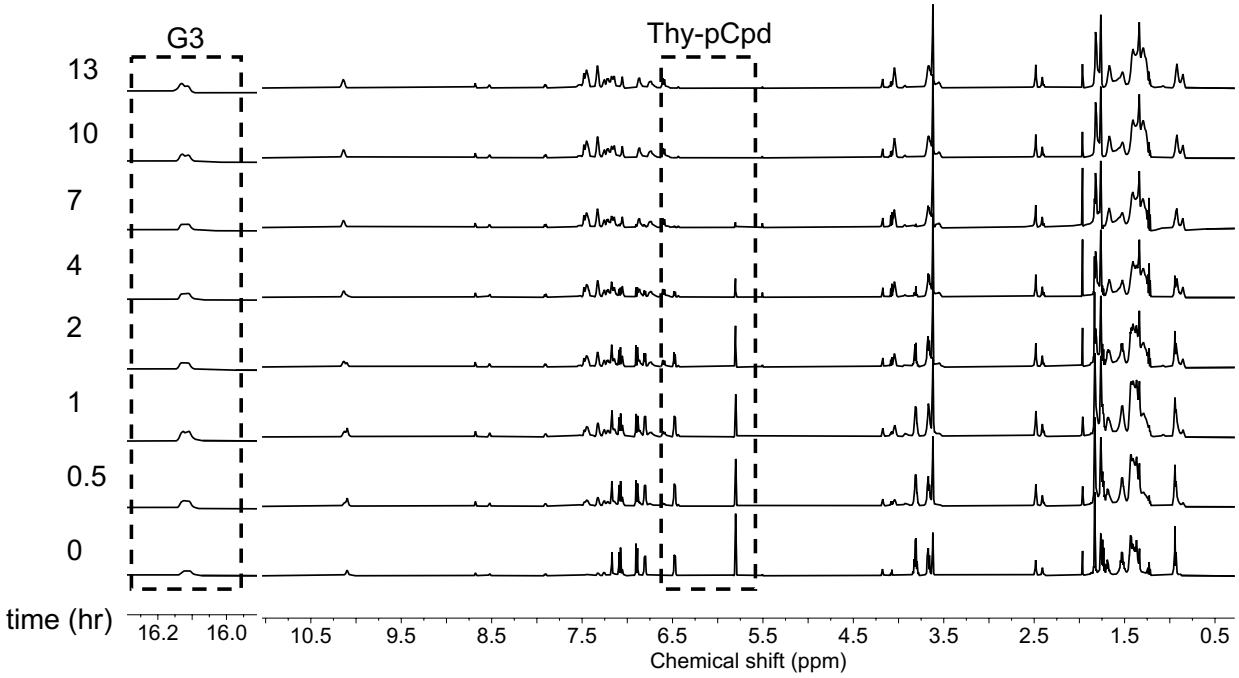

Figure 4. Polymerization progress of Thy-pCpd monitored by ^{1}H NMR spectroscopy in THF-d_8 (600 MHz). The signal within the left box corresponds to the benzylidene proton signal from the Grubbs initiator. The signals within the right box correspond to the aromatic protons of Thy-pCpd, showing the consumption of the monomer.

Thy-bearing pCpd was polymerized using a Grubbs' third generation initiator and terminated with a vinyl ether containing the alkyne-Pd PIC catalyst. The progress of the polymerization was monitored using ^{1}H NMR spectroscopy (**Figure 4**). The decreasing intensity of the monomer peaks compared to the catalyst peaks and the consistent benzylidene proton signal from the carbene specie at 16.09 ppm demonstrates the polymerization progress. The obtained ***cis*,*trans*-Thy-PPV** with Thy side-chains exhibits an M_n of 5.6 kDa ($Đ$ = 1.15). The successful terminal functionalization of the PPV with the Pd catalyst was confirmed by the ^{31}P NMR signal of the coordinated PEt_3 at 17.92 ppm which is consistent with PEt_3 signal in the small molecule compound (Figure S1).[45]

Upon UV irradiation at 365 nm using a hand-held UV lamp, the double bonds in the olefin backbone were transformed to the all-*trans* conformation from a *cis*,*trans* mixture (**Figure 5**a). We confirmed the successful isomerization by the large red-shift of the absorbance spectrum observed using UV-Vis spectroscopy. As shown in the Figure 5b, the maximum absorbance shifted

from 412 nm to 466 nm, indicating an extended conjugated backbone length upon the *cis*,*trans* to all-*trans* isomerization. At the same time, the fluorescence emission spectrum (Figure 5c) of the **all-*trans*-Thy-PPV** shows negligible changes compared to the fluorescence spectrum of the ***cis*,*trans*-Thy-PPV**. The apparent molecular weight of the **all-*trans*-Thy-PPV**, measured using GPC, also increased from 5.6 kDa to 9.3 kDa ($Đ$ = 1.27), which is expected because the isomerization converted the bent *cis* double bonds to *trans* double bonds thereby increasing the rigidity and ultimately the length of the polymer chain.[52, 59] The ^{1}H NMR spectrum in Figure 5d shows the effect of isomerization to the chemical shifts of the PPV protons with the conjugated backbone peaks converging (7.6-6.6 ppm) to signals associated with *trans*-vinylene protons.[60][29] Additionally, the signal corrsponding to the methylene groups attached to the oxygen atom on PPV's backbone significantly decrease around 3.5 ppm while the *trans* stereoisomer methylene peak around 4.2 ppm becomes more prominent. The amide proton of the Thy units, observed at around 9.5 ppm, shift downfield compared to the monomer N-H proton peak, indicating the self-association of the thymine units in $CDCl_3$. Due to the poor solubility of the **all-*trans*-Thy-PPV** in chloroform, an association constant could not be obtained. After mixing one equivalent of the DAP model compound *N*,*N*′-(pyridine-2,6-diyl)dibutyramide with the **all-*trans*-Thy-PPV** solution in THF, the dried mixture is soluble in chloroform, suggesting the formation of hydrogen bonds between the polymer and the model compound. By ^{1}H NMR spectroscopy, we observed a significant downfield shift of the Thy N-H proton when the sample was dissolved in $CDCl_3$.

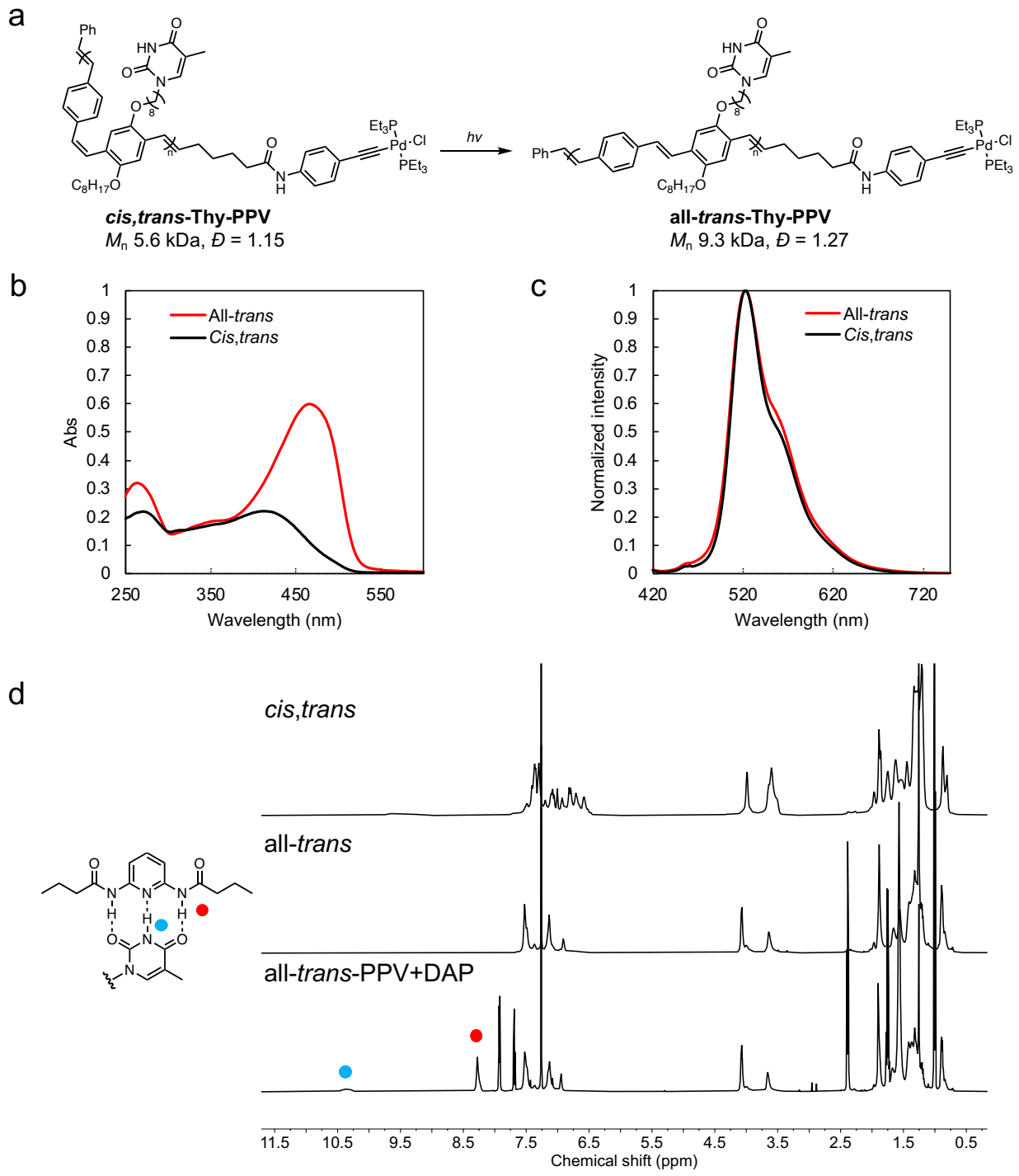

Figure 5. a) Schematic representation of the photoisomerization from ***cis,trans*-PPV** to **all-*trans*-PPV**. b) UV-Vis absorbance spectra and c) fluorescence spectra (excited at 420 nm) of Thy-PPV in THF before (*cis*,*trans*) and after (all-*trans*) UV irradiation at 365 nm. d) ^{1}H NMR spectra of PPV before (*cis*,*trans*), after (all-*trans*) UV irradiation, and **all-*trans*-PPV** with one eq. of DAP model compound *N*,*N*′-(pyridine-2,6-diyl)dibutyramide in $CDCl_3$.

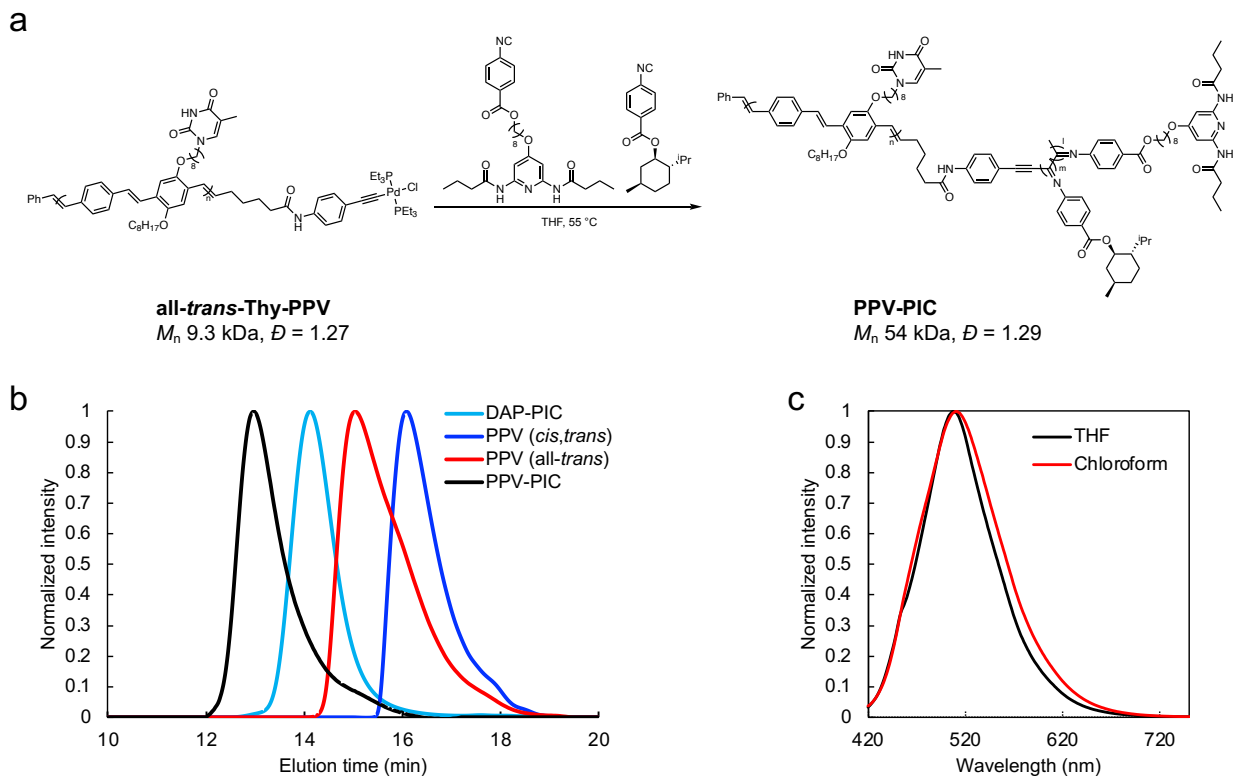

Figure 6. a) Schematic representation of the chain-extension from **all-*trans*-Thy-PPV** to **PPV-PIC.** b) GPC traces of **DAP-PIC**, ***cis*,*trans*-Thy-PPV**, **all-*trans*-Thy-PPV**, and **PPV-PIC** in THF. c) Fluorescence spectra (excited at 420 nm) of **PPV-PIC** in chloroform and THF.

2.3 Synthesis and characterization of PPV-PIC

Using the Pd terminated **all-*trans*-Thy-PPV** as the macroinitiator for polymerizing phenyl isocyanides, we prepared the **PPV-PIC** block copolymer. The sizes of the PIC and PPV polymer blocks were modeled computationally (Figure S2). We computed that a 10mer PPV is about 14 nm in length and a 100mer PIC composed of *L*-Men-PhNC is about 10 nm in length. Therefore, a DP of 100 was targeted with 10 DAP-PhNC units and 90 *L*-Men-PhNC units for the PPV-PIC block copolymer to ensure that the block lengths are similar in length for their successful folding. The polymerization was carried out in a similar fashion as described above for the homo-PIC. The obtained **PPV-PIC** block copolymer has a M_n of 54 kDa ($Đ$ = 1.29) and exhibits a single signal on GPC, indicating an efficient chain-extension from the **all-*trans*-Thy-PPV** (**Figure 6**).

As shown by the ^{1}H NMR spectra in **Figure 7**a, the **PPV-PIC** copolymer in THF-d_8 and $CDCl_3$ exhibit the characteristic signals of both the PPV and the PIC blocks. The UV-Vis spectrum

(Figure 3d) of **PPV-PIC** primarily shows the absorption features of the100mer PIC block because there are only ten repeat units for the PPV block. The helical secondary domain was confirmed by CD spectroscopy (Figure 3a and 3c), which shows the same spectra for **DAP-PIC** and **PPV-PIC** with major positive Cotton effects at around 360 nm and secondary negative Cotton effects at 250 nm, indicating a right-handed helix. The shift of the CD spectra in chloroform and THF observed for **DAP-PIC** was also observed for **PPV-PIC**, suggesting that the PIC block of the **PPV-PIC** copolymer has the same helical conformation as the **DAP-PIC**. The fluorescence emission spectra (Figure 6c) of **PPV-PIC** recorded in both solvents confirmed the flat conjugated backbone of the PPV block of **PPV-PIC**.

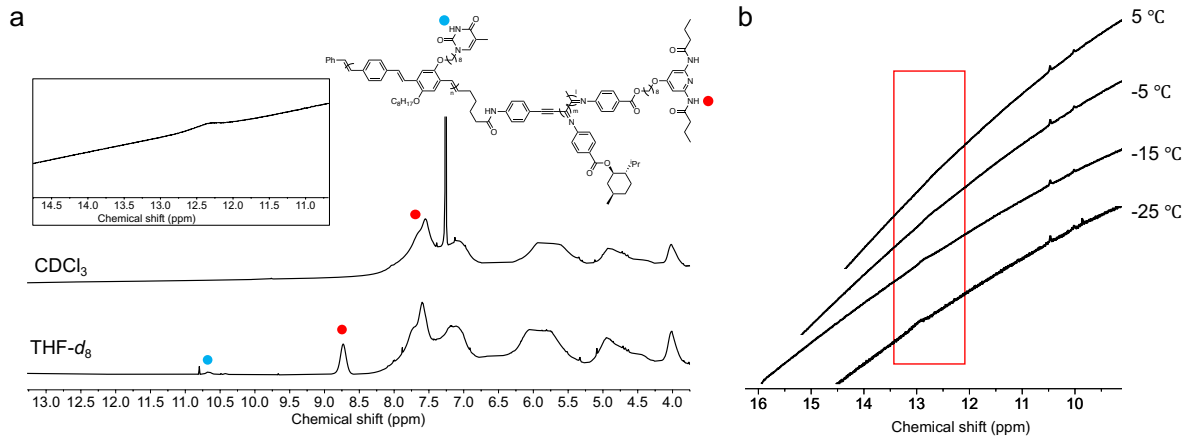

Figure 7. a) ^{1}H NMR spectra of **PPV-PIC** in (top) $CDCl_3$ and (bottom) THF-d_8. The inlet shows the very broad peak at 12.3 ppm. b) Partial ^{1}H NMR of **PPV-PIC** at 1 mg mL^{-1} in $CDCl_3$ at different temperatures (800 MHz).

2.4 Hydrogen bonding induced single-chain folding of PPV-PIC

With the side-chains functionalized with DAP and Thy in two different blocks, respectively, the **PPV-PIC** diblock copolymer is expected to form a folded single-chain nanoparticle with a well-defined 3D structure. We investigated the size of the copolymers as a function of solvents using DLS (**Table 1** and **Figure 8)**. Dissolving the polymer in chloroform, which favors the formation of hydrogen bonds, should yield a collapse of the block copolymer into a 3D structure, i.e. limiting the degree of freedoms for the block copolymer resulting in smaller sizes. In contrast, polymer collapse should not occur in THF which is a competitive solvent and disrupts hydrogen bonding. We investigated the sizes of the **DAP-PIC** and **all-*trans*-Thy-PPV** first to understand the size differences of the two individual polymers in THF and chloroform. The 100mer **DAP-**

PIC (1 mg mL^{-1}) exhibits a hydrodynamic diameter (D_h) of 10.5 ± 0.2 nm in THF and 10.5 ± 0.1 nm in chloroform, suggesting that the two sizes of **DAP-PIC** are the same in both solvents. **All-*trans*-Thy-PPV** forms an assembly of 142 ± 3 nm at 0.2 mg mL^{-1} in THF with no peaks in the small diameter region. By reducing the concentration to 0.1 mg mL^{-1}, two species were observed: 130 ± 2 nm and 11.1 ± 0.6 nm. The major peak at 130 nm indicates the tendency of **all-*trans*-Thy-PPV** to aggregate, even in THF. The peak in the smaller size region is close to the estimated size of a 10mer PPV suggesting the existence of a single polymer chain. In chloroform, **all-*trans*-Thy-PPV** (0.1 mg mL^{-1}) also exhibits two signals in its DLS profile, with sizes of 136 ± 9 nm and 11.4 ± 2.3 nm, suggesting that the sizes of **all-*trans*-Thy-PPV** polymer chain in THF and chloroform are similar. The measured D_h of **DAP-PIC** and **all-*trans*-Thy-PPV** suggests that the difference of chloroform and THF has negligible influences on the sizes of these two polymer chains.

Next, we measured the sizes of the **PPV-PIC** copolymer in THF and chloroform. **PPV-PIC** exhibits a D_h of 15.5 ± 0.5 nm in chloroform at a concentration of 1.0 mg mL^{-1}. The size suggests a folded polymer chain compared to the sizes of **DAP-PIC** and **all-*trans*-Thy-PPV**. The size was further confirmed to be 15.9 ± 0.2 nm by reducing the sample concentration to 0.5 mg mL^{-1}. Based on the association constant measured using **DAP-PIC** and *N*-hexylthymine, 50 equivalents of Thy are required to saturate over 90% of the DAP units on the polymer at 1.0 mg mL^{-1}. The measured size of **PPV-PIC** (1 mg mL^{-1} in chloroform) increased to 19.6 ± 0.8 nm by adding 50 equivalents of *N*-hexylthymine. The large increase of the D_h is strong evidence of unfolding of the **PPV-PIC** by disrupting the intramolecular hydrogen bonding interactions between DAP on PIC and Thy on PPV. The D_h of **PPV-PIC** in THF was measured to be 21.7 ± 0.9 nm, which is significantly larger than the size of **PPV-PIC** in chloroform and close to the value of the unfolded **PPV-PIC** and *N*-hexylthymine mixture in chloroform.

To further understand the folding and unfolding events, we carried out DOSY experiments for the polymer and its mixture with *N*-hexylthymine in $CDCl_3$. In $CDCl_3$ and at 25 °C, the **PPV-PIC** has a diffusion coefficient of $3.134 \bullet 10^{-10}$ m^2 s^{-1} while the **PPV-PIC** and *N*-hexylthymine mixture exhibits a smaller diffusion coefficient of $1.069 \bullet 10^{-10}$ m^2 s^{-1}. The decrease in diffusion indicates a larger particle size, suggesting the unfolding of the **PPV-PIC** block copolymer upon mixing with competing hydrogen-bonding molecules *N*-hexylthymine.

The hydrogen bonding interaction between DAP and Thy was studied by ^1H NMR spectroscopy. Considering the **PPV-PIC** block copolymer contains 10 Thy and 10 DAP units

distributed along the rigid backbone, only limited numbers of Thy-DAP pairs are able to form between the two blocks. The ^{1}H NMR spectrum of **PPV-PIC** (Figure 7a) at a high concentration (10 mg mL^{-1}) was taken in $CDCl_3$ and THF-d_8. In THF-d_8, the DAP amide and Thy proton signals both shifted downfield to 8.73 ppm and 10.66 ppm. This observation is consistent with the downfield shift of the amide protons of a previously reported DAP-containing PIC in THF-d_8.[51] In $CDCl_3$, the spectrum of **PPV-PIC** shows similar signals to the spectrum in THF-d_8, except the signal representing the DAP amide protons was found as a broad shoulder at 7.7 ppm. A very broad peak was observed at 12.3 ppm that can be assigned to the protons involved in the hydrogen bonding. Based on the comparison of the spectra in $CDCl_3$ and THF-d_8, we reasoned that the majority of the DAP and Thy units were not involved in hydrogen bonds in $CDCl_3$, with only a limited number of units associating strongly in an intramolecular fashion. No observable signal can be assigned to the hydrogen bonding protons for a **PPV-PIC** sample at 1 mg mL^{-1} in $CDCl_3$ at 25 ˚C. Cooling down the sample to -25 °C, however, allows for the detection of a very weak and broad signal at around 12.8 ppm matching the signal seen in the more concentrated sample (Figure 7b). These DLS and NMR spectroscopy studies reveal that the hydrogen bonding between DAP and Thy mediated a folding event of the **PPV-PIC** diblock copolymer.

Table 1. Hydrodynamic diameters measured by DLS

Sample	D_h **(nm) in THF**	D_h **(nm) in $CHCl_3$**
DAP-PIC	10.5 ± 0.2	10.5 ± 0.1
All-*trans*-Thy-PPV	11.1 ± 0.6	11.4 ± 2.3
PPV-PIC	21.7 ± 0.9	15.5 ± 0.5
PPV-PIC+Thy	NA	19.6 ± 0.8

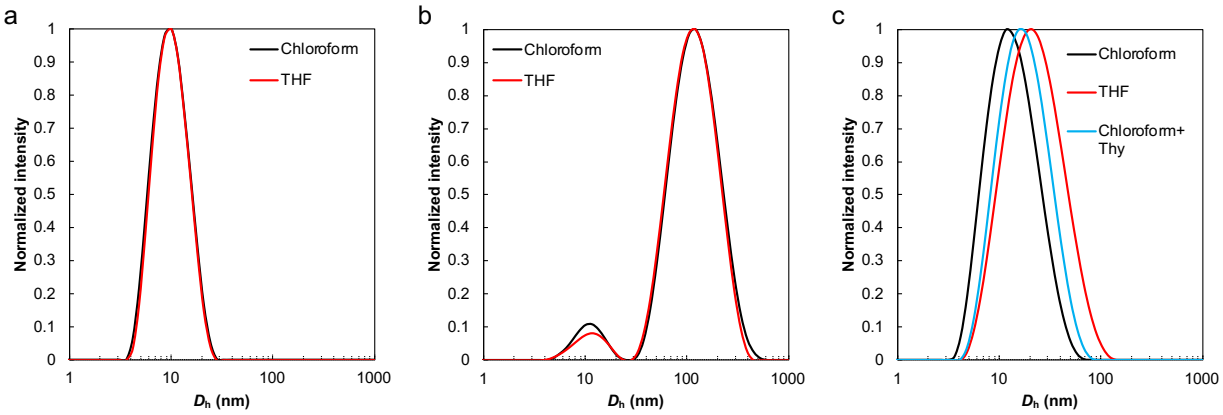

Figure 8. DLS profiles of a) **DAP-PIC**, b) ***cis,trans*-Thy-PPV**, and c) **PPV-PIC** in chloroform and THF.

3. Conclusion

In summary, we report the synthesis of side-chain functionalized **PPV-PIC** diblock copolymers featuring a sheet-like block and a helical block. This was accomplished by the living ROMP of thymine functionalized pCpds that can be terminated with a Pd-CTA for the macroinitiation of the helical DAP-PIC segment. The DAP-Thy association between the side-chains of the two polymer blocks directed the intramolecular folding of the sheet-helix to form a well-defined 3D structure in a hydrogen bonding favorable solvent. A 5-6 nm decrease in size of the sheet-helix copolymer induced by the intramolecular folding in chloroform was observed using DLS. The decrease in diffusion of the block copolymer upon unfolding was confirmed by DOSY experiments. The hydrogen bonding induced downfield shifts of the protons involved in the assemble as observed by ^{1}H NMR spectroscopy at 10 mg mL^{-1} and room temperature, as well as at 1 mg mL^{-1} at -25 °C.

This study presents a method to create hierarchically folded protein-mimicking structures using synthetic polymers with unique secondary structures. Similar methods can be used to create more complicated single chain structures with multiple domains of the same or different secondary structures.[4]

4. Experimental Section

Materials and instrumental: All chemicals were purchased from Sigma Aldrich, TCI, or Oakwood Chemical, and used as received unless otherwise indicated. GPC data was collected using a

Shimadzu pump coupled to a Shimadzu RI detector with THF as the eluent at a flow rate of 1 mL min^{-1} at ambient temperature. Poly(styrene) standards purchased from Agilent Technologies were used for column calibration. A set of Shodex GPC columns (KF-804 and KF-802.5) was used. M_w, M_n, and $Đ$ represent respectively the apparent weight-average molecular weight, apparent number-average molecular weight, and dispersity index. ^{1}H NMR and ^{13}C NMR spectra were recorded at 25 °C or temperatures as specified on a Bruker AVIII 400 MHz, a Bruker AV4 500 MHz, a Bruker AVIII 600 MHz, or a Bruker AV4 800 MHz spectrometer. All chemical shifts are reported in parts per million (ppm) with reference to solvent residual peaks. Mass spectra of samples in methanol were acquired with an Agilent 6224 Accurate-Mass TOF/LC/MS Spectrometer. CD spectra and UV-Vis spectra were obtained at 25 °C on a Jasco J-1500 Circular Dichroism Spectrometer. Fluorescence spectra were obtained at 25 °C on a Horiba PTI QM400 fluorometer. Hydrodynamic diameters of the prepared polymers were determined at 25 °C by DLS using a Malvern Zetasizer Nano. All samples were filtered using a 0.45 μm syringe filter before measurements. DOSY experiments were performed on a Bruker AVIII 600 MHz spectrometer at 25°C with samples prepared in $CDCl_3$, detailed parameters can be found in the SI.

*Compound **1***: 8-Bromooctanol (1.39 g, 6.66 mmol) and 4-formamidobenzoic acid (1.00 g, 6.06 mmol) were dissolved in DCM (50 mL). DMAP (0.148 g, 1.21 mmol) and EDCI (2.32 g, 12.11 mmol) were added to the reaction mixture. The reaction was stirred overnight at room temperature. Then, the reaction mixture was washed using 10% w/w citric acid, 10% w/w aqueous solution of $NaHCO_3$, and saturated brine. The organic layer was dried with Na_2SO_4 and the solvent was removed under reduced pressure. The compound was purified using silica gel column chromatography (hexane/EtOAc 3:2, v/v) to obtain a white solid (1.52 g, yield 73%). ^{1}H NMR (500 MHz, $CDCl_3$, δ ppm): 8.85 (d, J = 11.0 Hz, 0.4H), 8.43 (s, 1H), 8.04 (m, 2H), 7.66 (s, 0.6H), 7.64 (d, J = 8.5 Hz, 1H), 7.14 (d, J = 8.5 Hz, 1H), 4.30 (m, 2H), 3.52 (t, J = 6.5 Hz, 0.8H), 3.40 (t, J = 7 Hz, 1.2H), 1.85 (m, 1.2H), 1.76 (m, 2.8H), 1.44 (m, 4H), 1.35 (m, 4H); ^{13}C NMR (126 MHz, $CDCl_3$, δ ppm): 166.1, 165.9, 161.9, 159.0, 140.9, 131.5, 130.9, 126.5, 119.1, 117.2, 65.1, 45.2, 34.0, 32.8, 32.7, 32.6, 29.10, 29.07, 28.8, 28.67, 28.64, 28.1, 26.8, 25.9. HRMS(+ESI): $C_{16}H_{22}BrNO_3$, calculated 735.1441 $[2M+Na]^+$, found 735.1445.

*Compound **2***: DAP-OH (300 mg, 1.13 mmol), compound **1** (423 mg, 1.19 mmol), and K_2CO_3 (313 mg, 2.26 mmol) were dissolved in MeCN (50 mL). The reaction was stirred for two days at 80 °C. The reaction mixture was condensed. Water was added and the mixture was extracted with DCM

(50 mL x 3). The combined organic phases were dried with Na_2SO_4 and the solvent was removed under reduced pressure. The compound was purified using silica gel column chromatography (hexane/EtOAc 1:1 to 3:4, v/v) to obtain a white solid (354 mg, yield 58%). ^{1}H NMR (600 MHz, $CDCl_3$, δ ppm): 8.83 (m, 0.3H), 8.43 (s, 0.6H), 8.03 (m, 2H), 7.70 (m, J = 6.0 Hz, 2H), 7.63 (br, 0.55H), 7.52 (m, J = 6.0 Hz, 2H) , 7.27 (m, 0.45H), 7.16 (t, J = 6.6 Hz, 0.7H), 4.33 (m, 2H), 4.01 (t, J = 6.3 Hz, 2H), 2.36 (t, J = 7.5 Hz, 4H), 1.75 (m, 8H), 1.50-1.35 (m, 6H), 1.01 (t, J = 6.9 Hz, 6H); ^{13}C NMR (151 MHz, $CDCl_3$, δ ppm): 171.8, 159.1, 131.5, 130.8, 126.9, 126.4, 119.1, 117.18, 117.15, 96.2, 68.7, 68.6, 65.2, 39.8, 28.92, 28.88, 28.85, 28.83, 28.4, 28.3, 26.1, 25.9, 25.7, 18.82, 18.79, 13.7. HRMS(+ESI): $C_{29}H_{40}N_4O_6$, calculated 541.3021 $[M+H]^+$, found 541.3073.

*Compound **3***: Compound **2** (254 mg, 0.47 mmol) and triethylamine (238 mg, 2.35 mmol) were dissolved in dry DCM (30 mL) and cooled to 0 °C under an argon atmosphere. $POCl_3$ (108 mg, 0.71 mmol) was added using a syringe. The reaction was stirred for two hours at 0 °C and then moved to ambient temperature and stirred for an additional 16 hours. The reaction was quenched using 10% w/w aqueous solution of $NaHCO_3$ and was washed using 10% w/w aqueous solution of $NaHCO_3$ and brine. The organic phase was dried with Na_2SO_4. The product was purified using silica gel column chromatography (hexane/EtOAc 2:1, v/v) to obtain a yellow sticky solid (201 mg, yield 82%). ^{1}H NMR (600 MHz, $CDCl_3$, δ ppm): 8.11 (d, J = 7.8 Hz, 2H), 7.60-7.45 (br, 2H), 7.55 (s, 2H), 7.47 (d, J = 8.4 Hz, 2H), 4.36 (t, J = 6.6 Hz, 2H), 4.06, (t, J = 6.3 Hz, 2H) 2.36 (t, J = 7.5 Hz, 4H), 1.82-1.74 (m, 4H), 1.78 (m, 4H), 1.50-1.43 (m, 4H), 1.42-1.37 (m, 4H), 1.03 (t, J = 7.5 Hz, 6H); ^{13}C NMR (151 MHz, $CDCl_3$, δ ppm): 171.5, 169.1, 166.9, 165.1, 150.3, 131.4, 130.8, 126.5, 96.1, 68.4, 65.7, 39.8, 29.13, 29.10, 28.8, 28.6, 25.9, 25.8, 18.7, 13.7. HRMS(+ESI): $C_{29}H_{38}N_4O_5$, calculated 523.2915 $[M+H]^+$, found 523.2920.

*Compound **4***: Dioctyloxy pCpd[26] (460 mg, 1.00 mmol) was dissolved in dry DCM (40 mL) and cooled to -78 °C. BBr_3 (544 mg, 2.17 mmol) in DCM (2.17 mL) was added using a syringe pump over a period of ten minutes. After the addition, the reaction was warmed up to room temperature and stirred for three hours. The reaction was quenched using DI water and extracted using DCM. The organic phase was dried with Na_2SO_4. The product was purified using silica gel column chromatography (DCM) to obtain a white powder (210 mg, yield 60%). ^{1}H NMR (400 MHz, $CDCl_3$, δ ppm): 7.33 (d, J = 9.6 Hz, 1H) , 7.15 (d, J = 10.0 Hz, 1H), 7.04 (d, J = 8.4 Hz, 1H), 6.92 (d, J = 10.4 Hz, 1H), 6.85 (d, J = 10.0 Hz, 1H), 6.82 (d, J = 8.8 Hz, 1H), 6.60 (d, J = 8.0 Hz, 1H), 6.46 (d, J = 7.6 Hz, 1H), 4.26 (s, 1H), 3.87-3.74 (m, 2H), 1.75 (m, 2H), 1.47 (m, 2H), 1.42-1.29

(m, 8H), 0.92 (t, J = 6.8 Hz, 1H); ^{13}C NMR (151 MHz, $CDCl_3$, δ ppm): 152.5, 148.0, 139.8, 138.6, 137.3, 135.6, 134.4, 132.2, 131.6, 131.2, 128.4, 128.0, 126.2, 124.3, 124.1, 118.8, 69.3, 31.9, 29.6, 29.4, 29.3, 26.2, 22.7, 14.1. HRMS(+ESI): $C_{24}H_{28}O_2$, calculated 371.1982 $[M+Na]^+$, found 371.2002.

*Compound **5***: Compound **4** (210 mg, 0.60 mmol), 1,8-dibromooctane (492 mg, 1.81 mmol), and K_2CO_3 (167 mg, 1.21 mmol) were dissolved in MeCN (15 mL). The reaction was stirred for 16 hours at 80 °C. The reaction mixture was condensed. Water was added and the mixture was extracted with DCM (20 mL x 3). The combined organic phases were dried with Na_2SO_4 and the solvent was removed under reduced pressure. The compound was then purified using silica gel column chromatography (hexane to hexane/DCM, 1:1, v/v) to obtain a white solid (178 mg, yield 48%). ^{1}H NMR (600 MHz, $CDCl_3$, δ ppm): 7.11 (d, J = 10.2 Hz, 2H), 6.90 (d, J = 10.2 Hz, 2H), 6.81 (m, 2H), 6.49 (d, J = 9.0 Hz, 2H), 5.78 (s, 2H), 3.83-3.73 (m, 4H), 3.42 (d, J = 6.9 Hz, 2H), 1.87 (m, 2H), 1.72 (m, 2H), 1.46-1.25 (m, 18H), 0.90 (d, J = 6.9 Hz, 3H); ^{13}C NMR (151 MHz, $CDCl_3$, δ ppm): 152.4, 152.3, 138.3, 138.2, 135.6, 135.5, 134.4, 131.3, 127.5, 127.5, 127.3, 120.4, 120.3, 69.13, 69.07, 34.0, 32.8, 31.9, 29.62, 29.57, 29.4, 29.3, 29.2, 28.7, 28.1, 26.2, 26.1, 22.7, 14.1. HRMS(+ESI): $C_{32}H_{43}BrO_2$, calculated 541.2504 $[M+H]^+$, found 541.2458.

*Compound **6***: Compound **5** (72 mg, 0.13 mmol), thymine (84 mg, 0.67 mmol), and Cs_2CO_3 (87 mg, 0.27 mmol) were dissolved in DMF (3 mL). The reaction was stirred for 15 hours at 60 °C. The reaction mixture was condensed. Water was added and the mixture and was extracted with DCM (10 mL x 3). The combined organic phases were dried with Na_2SO_4 and the solvent was removed under reduced pressure. The compound was purified using silica gel column chromatography (hexane/EtOAc, 3:2, v/v) to obtain a white sticky solid (39 mg, yield 50%). ^{1}H NMR (600 MHz, $CDCl_3$, δ ppm): 8.05 (s, 1H), 7.11 (d, J = 9.6 Hz, 2H), 6.96 (d, J = 1.2 Hz, 1H), 6.90 (dd, J_1 = 10.2 Hz, J_2 = 3.0 Hz, 2H), 6.80 (t, J = 7.5 Hz, 2H), 6.48 (d, J = 7.8 Hz, 2H), 5.77 (s, 2H), 3.82-3.78 (m, 2H), 3.76-3.72 (m, 2H), 3.68 (t, J = 7.5 Hz, 2H), 1.92 (d, J = 1.2 Hz, 3H), 1.75-1.65 (m, 6H), 1.47-1.41 (m, 4H), 1.37-1.26 (m, 14H), 0.89 (d, J = 6.9 Hz, 3H); ^{13}C NMR (151 MHz, $CDCl_3$, δ ppm): 163.8, 152.4, 152.3, 150.6, 140.4, 138.3, 138.1, 135.55, 135.53, 134.4, 131.3, 127.54, 127.47, 127.30, 127.28, 120.4, 120.3, 110.5, 77.2, 77.0, 76.8, 69.1, 69.0, 48.6, 31.9, 29.62, 29.55, 29.4, 29.3, 29.24, 29.16, 29.1, 26.4, 26.2, 26.1, 22.7, 14.1, 12.3. HRMS(+ESI): $C_{37}H_{48}N_2O_4$, calculated 607.3506 $[M+Na]^+$, found 607.3553.

*Synthesis of **DAP-PIC***: Pd catalyst (0.49 mg, 0.78 μmol), *L*-Men-PhNC (20.0 mg, 70.1 μmol), and DAP-PhNC (4.07 mg, 7.79 μmol) were dissolved in THF (0.78 mL) in a Schlenk flask. Three freeze-pump-thaw circles were applied to degas the reaction mixture. The flask was then transferred to an oil bath and the reaction mixture was stirred at 55 °C for 24 hours. The solvent was removed under reduced pressure. The crude product was dissolved in a minimal amount of THF and was precipitated in methanol. The dissolution and precipitation procedure was repeated three times and the product was obtained by filtration and dried under vacuum as a brown solid (23 mg, yield 94%).

*Synthesis of **cis,trans-PPV-Thy***: In a N_2 filled glovebox, Thy-pCpd (compound **6**, 26.0 mg, 44.5 μmol) was dissolved in THF (0.2 mL) and Grubbs' third generation initiator (3.93 mg, 4.45 μmol) dissolved in THF (0.245 mL) was added to the solution. The flask was heated to 50 °C and stirred until completion. After the reaction was completed, Pd-CTA (11.3 mg, 17.8 μmol) was added and allowed to stir at room temperature over a period of 12 hours. The polymer solution was reprecipitated using cold hexanes (x1) and methanol (x3), affording a red solid (26 mg, yield 89%).

*Synthesis of **PPV-PIC***: **All-*trans*-Thy-PPV** (9.60 mg, 1.71 μmol), *L*-Men-PhNC (44.0 mg, 0.154 mmol), and DAP-PhNC (8.96 mg, 17.1 μmol) were dissolved in THF (1.71 mL) in a Schlenk flask. Three freeze-pump-thaw circles were applied to degas the reaction mixture. The flask was then transferred to an oil bath and the reaction mixture was stirred at 55 °C for 24 hours. The solvent was removed under reduced pressure. The crude product was dissolved in a minimal amount of THF and precipitated in cold methanol (x3). The dissolution and precipitation procedure was repeated three times and the product was obtained by centrifugation and dried under vacuum as a reddish brown solid (59 mg, yield 94%).

Supporting Information

Supporting Information is available from the Wiley Online Library or from the author.

Acknowledgements

The authors acknowledge financial support from the National Science Foundation under award number CHE 2203929.

Received: ((will be filled in by the editorial staff))
Revised: ((will be filled in by the editorial staff))
Published online: ((will be filled in by the editorial staff))

References

[1] M. Heim, L. Römer, T. Scheibel, *Chem. Soc. Rev.* **2010**, *39*, 156.
[2] W. S. Horne, T. N. Grossmann, *Nat. Chem.* **2020**, *12*, 331.
[3] R. W. Newberry, R. T. Raines, *ACS Chem. Biol.* **2019**, *14*, 1677.
[4] H. Frisch, B. T. Tuten, C. Barner-Kowollik, *Isr. J. Chem.* **2020**, *60*, 86.
[5] J. Chen, K. Li, J. S. L. Shon, S. C. Zimmerman, *J. Am. Chem. Soc.* **2020**, *142*, 4565.
[6] J. J. Piane, L. E. Chamberlain, S. Huss, L. T. Alameda, A. C. Hoover, E. Elacqua, *ACS Catalysis* **2020**, *10*, 13251.
[7] J. Chen, K. Li, S. E. Bonson, S. C. Zimmerman, *J. Am. Chem. Soc.* **2020**, *142*, 13966.
[8] Y. Liu, S. Pujals, P. J. M. Stals, T. Paulöhrl, S. I. Presolski, E. W. Meijer, L. Albertazzi, A. R. A. Palmans, *J. Am. Chem. Soc.* **2018**, *140*, 3423.
[9] T. Terashima, T. Mes, T. F. A. De Greef, M. A. J. Gillissen, P. Besenius, A. R. A. Palmans, E. W. Meijer, *J. Am. Chem. Soc.* **2011**, *133*, 4742.
[10] A. Sanchez-Sanchez, S. Akbari, A. Etxeberria, A. Arbe, U. Gasser, A. J. Moreno, J. Colmenero, J. A. Pomposo, *ACS Macro Lett.* **2013**, *2*, 491.
[11] N. D. Knöfel, H. Rothfuss, J. Willenbacher, C. Barner-Kowollik, P. W. Roesky, *Angew. Chem. Int. Ed.* **2017**, *56*, 4950.
[12] H. Rothfuss, N. D. Knöfel, P. W. Roesky, C. Barner-Kowollik, *J. Am. Chem. Soc.* **2018**, *140*, 5875.
[13] A. B. Benito, M. K. Aiertza, M. Marradi, L. Gil-Iceta, T. Shekhter Zahavi, B. Szczupak, M. Jiménez-González, T. Reese, E. Scanziani, L. Passoni, M. Matteoli, M. De Maglie, A. Orenstein, M. Oron-Herman, G. Kostenich, L. Buzhansky, E. Gazit, H.-J. Grande, V. Gómez-Vallejo, J. Llop, I. Loinaz, *Biomacromolecules* **2016**, *17*, 3213.
[14] J. Willenbacher, K. N. R. Wuest, J. O. Mueller, M. Kaupp, H.-A. Wagenknecht, C. Barner-Kowollik, *ACS Macro Lett.* **2014**, *3*, 574.
[15] P. Wang, H. Pu, J. Ge, M. Jin, H. Pan, Z. Chang, D. Wan, *Mater. Lett.* **2014**, *132*, 102.
[16] D. N. F. Bajj, M. V. Tran, H.-Y. Tsai, H. Kim, N. R. Paisley, W. R. Algar, Z. M. Hudson, *ACS Applied Nano Materials* **2019**, *2*, 898.
[17] A. P. P. Kröger, J. M. J. Paulusse, *J. Controlled Release* **2018**, *286*, 326.
[18] A. P. P. Kröger, M. I. Komil, N. M. Hamelmann, A. Juan, M. H. Stenzel, J. M. J. Paulusse, *ACS Macro Lett.* **2019**, *8*, 95.
[19] C.-C. Cheng, D.-J. Lee, Z.-S. Liao, J.-J. Huang, *Polym. Chem.* **2016**, *7*, 6164.
[20] A. P. P. Kröger, N. M. Hamelmann, A. Juan, S. Lindhoud, J. M. J. Paulusse, *ACS Appl. Mater. Interfaces* **2018**, *10*, 30946.
[21] R. Gracia, M. Marradi, G. Salerno, R. Pérez-Nicado, A. Pérez-San Vicente, D. Dupin, J. Rodriguez, I. Loinaz, F. Chiodo, C. Nativi, *ACS Macro Lett.* **2018**, *7*, 196.
[22] C. K. Lyon, A. Prasher, A. M. Hanlon, B. T. Tuten, C. A. Tooley, P. G. Frank, E. B. Berda, *Polym. Chem.* **2015**, *6*, 181.
[23] A. M. Hanlon, C. K. Lyon, E. B. Berda, *Macromolecules* **2016**, *49*, 2.
[24] G. M. t. Huurne, A. R. A. Palmans, E. W. Meijer, *CCS Chemistry* **2019**, *1*, 64.

[25] M. Milton, R. Deng, A. Mann, C. Wang, D. Tang, M. Weck, *Acc. Chem. Res.* **2021**, *54*, 2397.
[26] E. Elacqua, K. B. Manning, D. S. Lye, S. K. Pomarico, F. Morgia, M. Weck, *J. Am. Chem. Soc.* **2017**, *139*, 12240.
[27] J. Chen, J. Wang, K. Li, Y. Wang, M. Gruebele, A. L. Ferguson, S. C. Zimmerman, *J. Am. Chem. Soc.* **2019**, *141*, 9693.
[28] D. Chao, X. Jia, B. Tuten, C. Wang, E. B. Berda, *Chem. Commun.* **2013**, *49*, 4178.
[29] P. G. Frank, B. T. Tuten, A. Prasher, D. Chao, E. B. Berda, *Macromol. Rapid Commun.* **2014**, *35*, 249.
[30] J. He, L. Tremblay, S. Lacelle, Y. Zhao, *Soft Matter* **2011**, *7*, 2380.
[31] B. T. Tuten, D. Chao, C. K. Lyon, E. B. Berda, *Polym. Chem.* **2012**, *3*, 3068.
[32] O. Altintas, J. Willenbacher, K. N. R. Wuest, K. K. Oehlenschlaeger, P. Krolla-Sidenstein, H. Gliemann, C. Barner-Kowollik, *Macromolecules* **2013**, *46*, 8092.
[33] E. J. Foster, E. B. Berda, E. W. Meijer, *J. Am. Chem. Soc.* **2009**, *131*, 6964.
[34] E. B. Berda, E. J. Foster, E. W. Meijer, *Macromolecules* **2010**, *43*, 1430.
[35] T. Mes, R. van der Weegen, A. R. A. Palmans, E. W. Meijer, *Angew. Chem. Int. Ed.* **2011**, *50*, 5085.
[36] O. Altintas, E. Lejeune, P. Gerstel, C. Barner-Kowollik, *Polym. Chem.* **2012**, *3*, 640.
[37] N. Hosono, M. A. J. Gillissen, Y. Li, S. S. Sheiko, A. R. A. Palmans, E. W. Meijer, *J. Am. Chem. Soc.* **2013**, *135*, 501.
[38] T. S. Fischer, D. Schulze-Sünninghausen, B. Luy, O. Altintas, C. Barner-Kowollik, *Angew. Chem. Int. Ed.* **2016**, *55*, 11276.
[39] J. P. Cole, J. J. Lessard, K. J. Rodriguez, A. M. Hanlon, E. K. Reville, J. P. Mancinelli, E. B. Berda, *Polym. Chem.* **2017**, *8*, 5829.
[40] T. Terashima, T. Sugita, K. Fukae, M. Sawamoto, *Macromolecules* **2014**, *47*, 589.
[41] E. A. Appel, J. Dyson, J. del Barrio, Z. Walsh, O. A. Scherman, *Angew. Chem. Int. Ed.* **2012**, *51*, 4185.
[42] J. Willenbacher, B. V. K. J. Schmidt, D. Schulze-Suenninghausen, O. Altintas, B. Luy, G. Delaittre, C. Barner-Kowollik, *Chem. Commun.* **2014**, *50*, 7056.
[43] J. Willenbacher, O. Altintas, P. W. Roesky, C. Barner-Kowollik, *Macromol. Rapid Commun.* **2014**, *35*, 45.
[44] R. Deng, M. Milton, S. K. Pomarico, M. Weck, *Polym. Chem.* **2019**, *10*, 5087.
[45] E. Elacqua, A. Croom, D. S. Lye, M. Weck, *J. Polym. Sci., Part A: Polym. Chem.* **2017**, *55*, 2991.
[46] S. K. Pomarico, D. S. Lye, E. Elacqua, M. Weck, *Polym. Chem.* **2018**, *9*, 5655.
[47] E. Elacqua, A. Croom, K. B. Manning, S. K. Pomarico, D. Lye, L. Young, M. Weck, *Angew. Chem. Int. Ed.* **2016**, *55*, 15873.
[48] S. K. Pomarico, C. Wang, M. Weck, *Macromol. Rapid Commun.* **2020**, *41*, e1900324.
[49] R. Deng, C. Wang, M. Milton, D. Tang, A. D. Hollingsworth, M. Weck, *Polym. Chem.* **2021**, *12*, 4916.
[50] C. Wang, M. Weck, *Macromol. Rapid Commun.* **2021**, *42*, 2100368.
[51] C. Wang, R. Deng, M. Weck, *Macromolecules* **2023**, *56*, 3507.
[52] A. Mann, M. D. Hannigan, M. Weck, *Macromol. Chem. Phys.* **2023**, *224*, 2200397.
[53] A. Mann, C. Wang, B. L. Dumlao, M. Weck, *ACS Macro Lett.* **2024**, *13*, 112.
[54] Y.-X. Xue, J.-L. Chen, Z.-Q. Jiang, Z. Yu, N. Liu, J. Yin, Y.-Y. Zhu, Z.-Q. Wu, *Polym. Chem.* **2014**, *5*, 6435.

[55] C. R. South, K. C. F. Leung, D. Lanari, J. F. Stoddart, M. Weck, *Macromolecules* **2006**, *39*, 3738.
[56] K. P. Nair, J. M. Pollino, M. Weck, *Macromolecules* **2006**, *39*, 931.
[57] J. M. Pollino, L. P. Stubbs, M. Weck, *J. Am. Chem. Soc.* **2004**, *126*, 563.
[58] C. Reichardt, *Chem. Rev.* **1994**, *94*, 2319.
[59] A. Mann, M. Weck, *ACS Macro Lett.* **2022**, 1055.
[60] C.-Y. Yu, M. L. Turner, *Angew. Chem. Int. Ed.* **2006**, *45*, 7797.

Folded polymer architectures featuring both secondary and well-defined 3D structures that mimic proteins have been an unfulfilled goal. Here, a synthetic block copolymer with a carbon-based backbone bearing two distinct secondary structures, helices and sheets, composed of poly(isocyanide)s and poly(*p*-phenylene vinylene)s, folds into a defined 3D architecture through hydrogen bonding mediated side-chain assemblies.

Chengyuan Wang, Arielle Mann, Regina H. Garvey, Bianca L. Dumlao, Matthew D. Hannigan, and Marcus Weck*

Folded Well-Defined 3D Architecture from Synthetic Helical and Sheet-Like Polymers

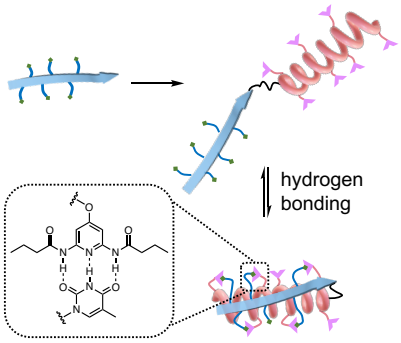

Supporting Information

Folded Well-Defined 3D Architecture from Synthetic Helical and Sheet-Like Polymers

*Chengyuan Wang, Arielle Mann, Regina H. Garvey, Bianca L. Dumlao, Matthew D. Hannigan, and Marcus Weck**

Department of Chemistry and Molecular Design Institute, New York University, 100 Washington Square East, New York, NY 10003

E-mail: mw125@nyu.edu

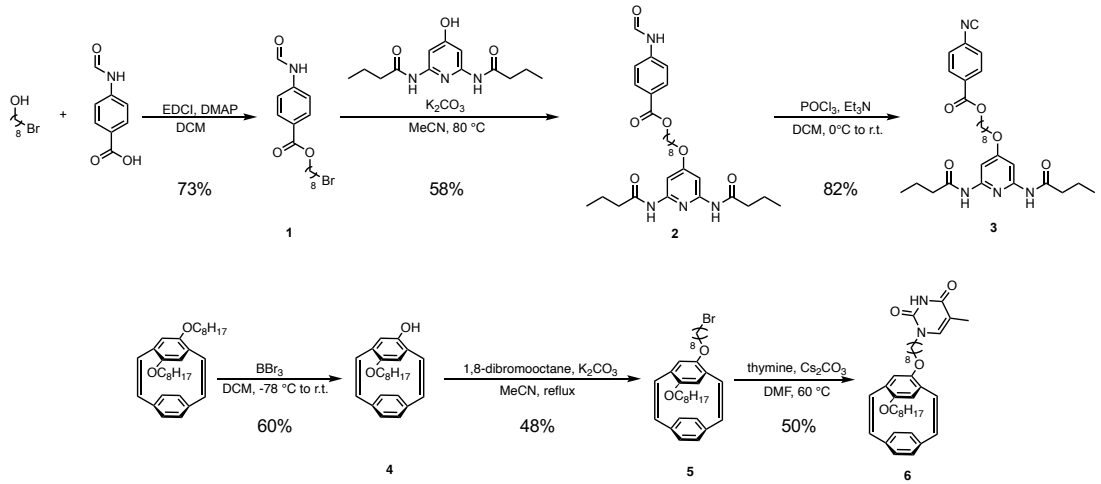

Synthetic routes towards DAP-PhNC and Thy-pCpd.

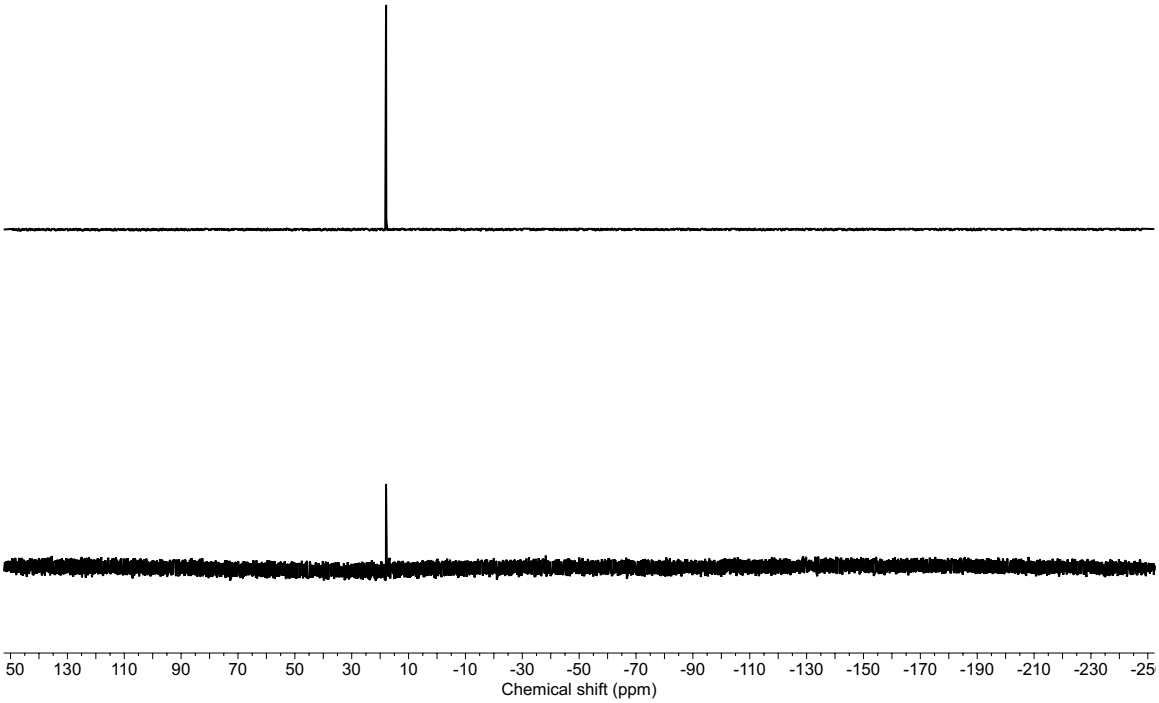

Figure S1. ^{31}P NMR spectra of CTA-Pd (top) and Thy-PPV (bottom) showing the signal from PEt_3 ligand at 17.92 ppm.

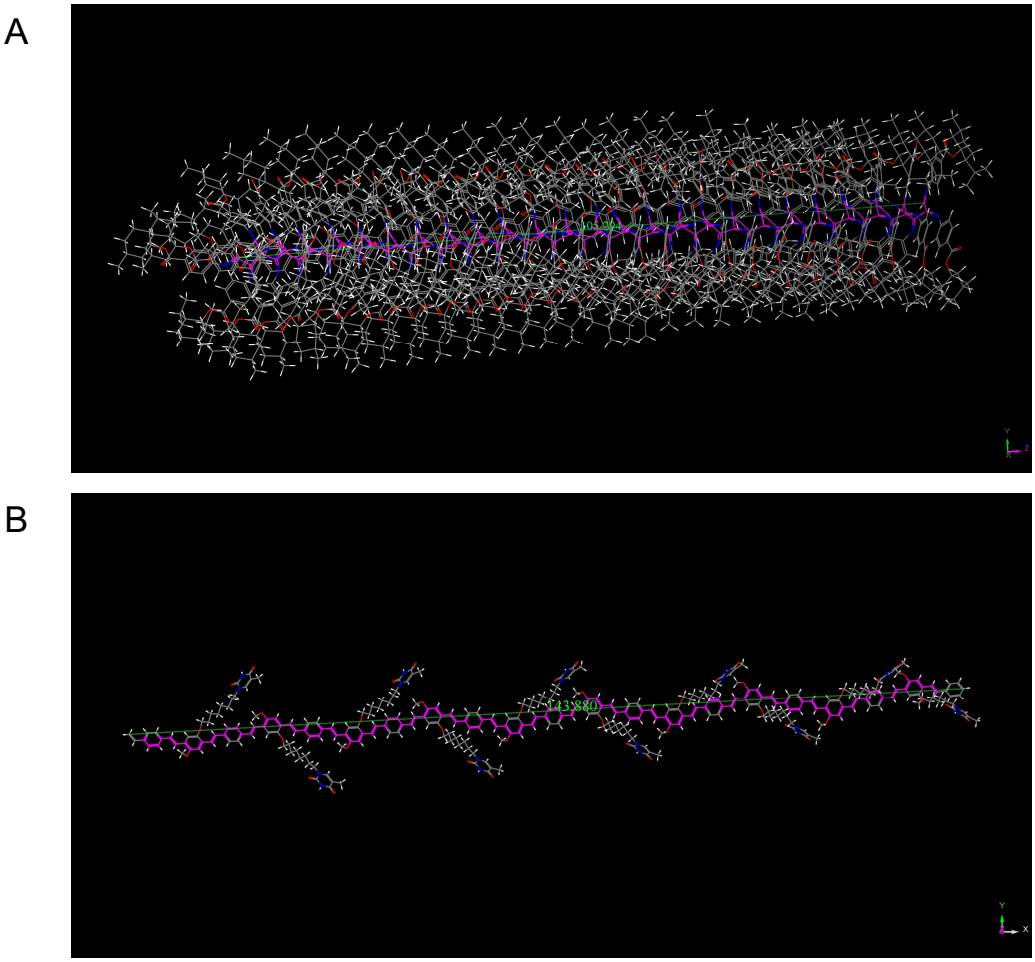

Figure S2. Estimated polymer chain sizes of (A) PIC 100mer and (B) PPV10mer based on single chain modeling using COMPASSII forcefield for geometry optimization in Materials Studio (unit Å).

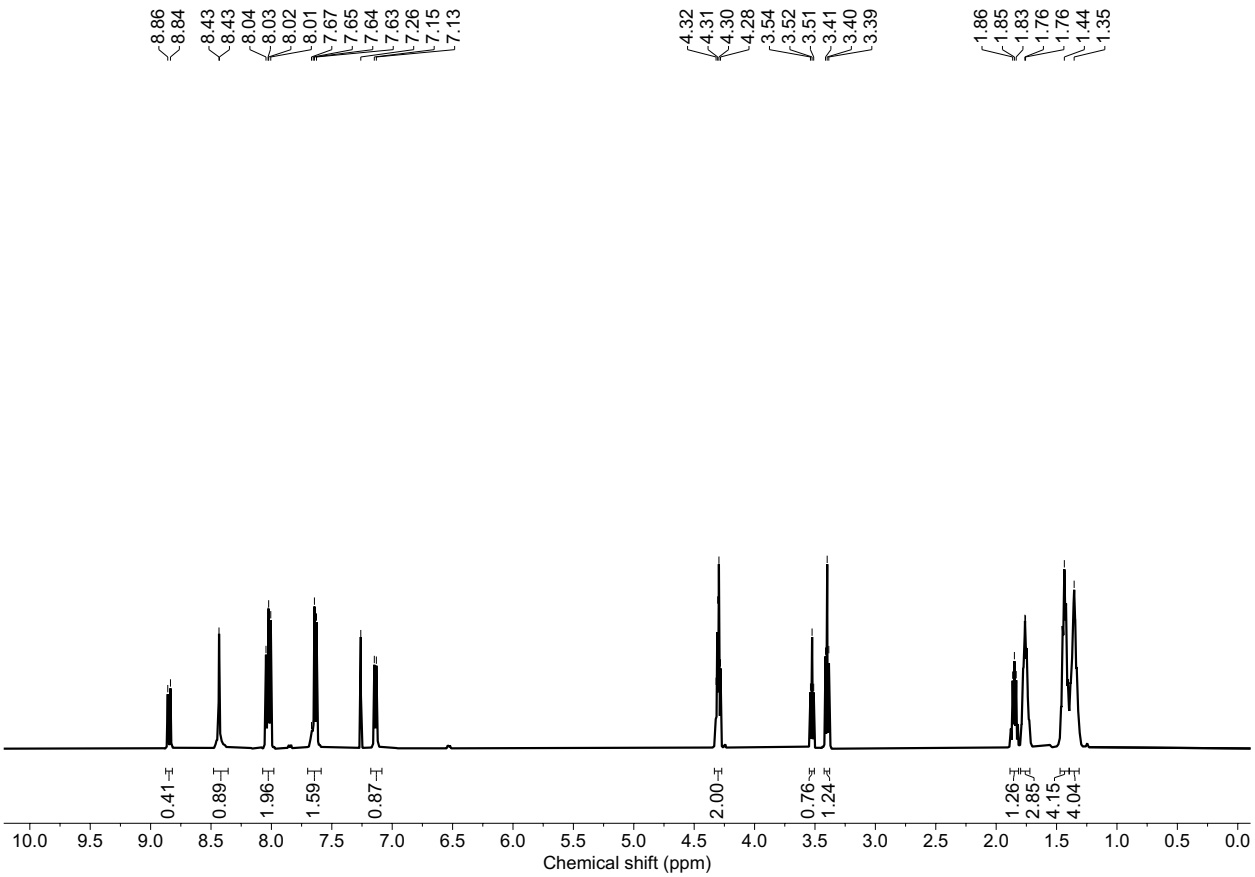

Figure S3. ^{1}H NMR spectrum of compound **1** in $CDCl_3$ (500 MHz).

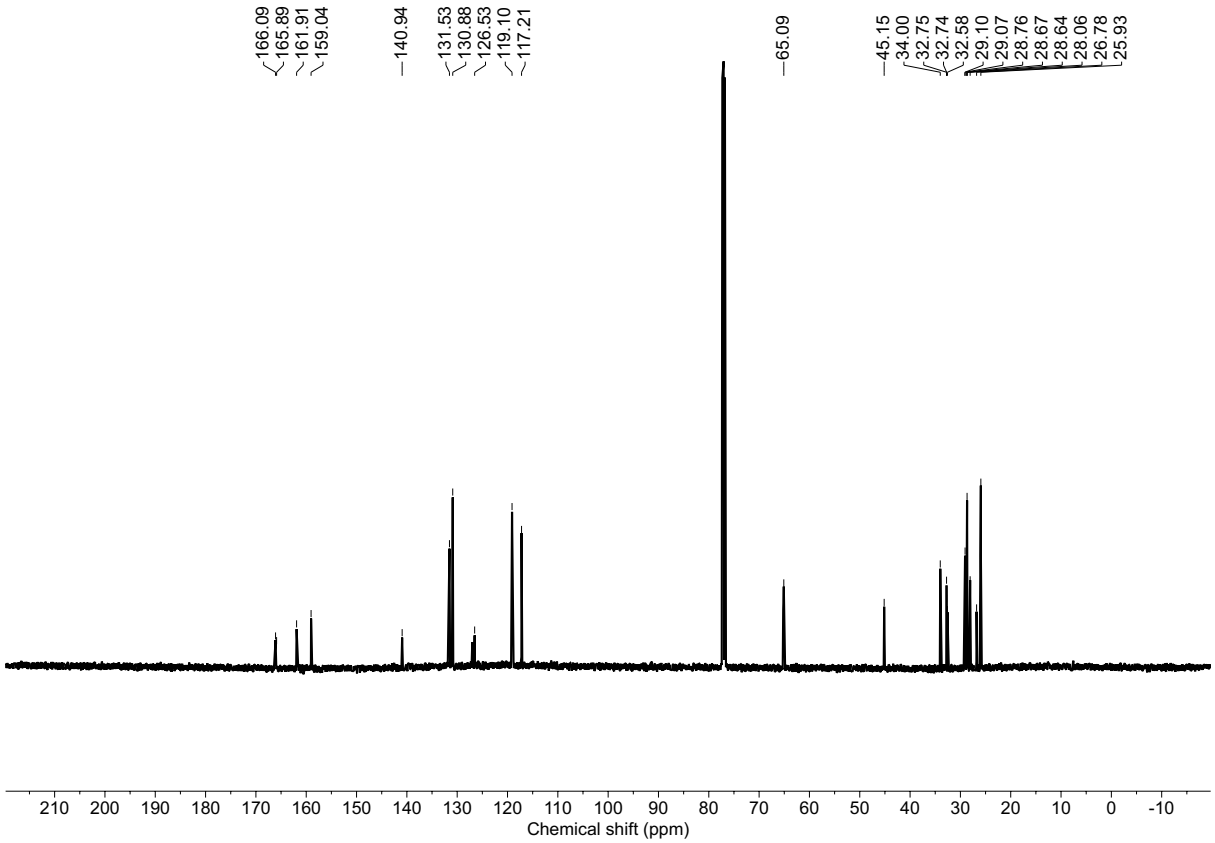

Figure S4. ^{13}C NMR spectrum of compound **1** in $CDCl_3$ (126 MHz).

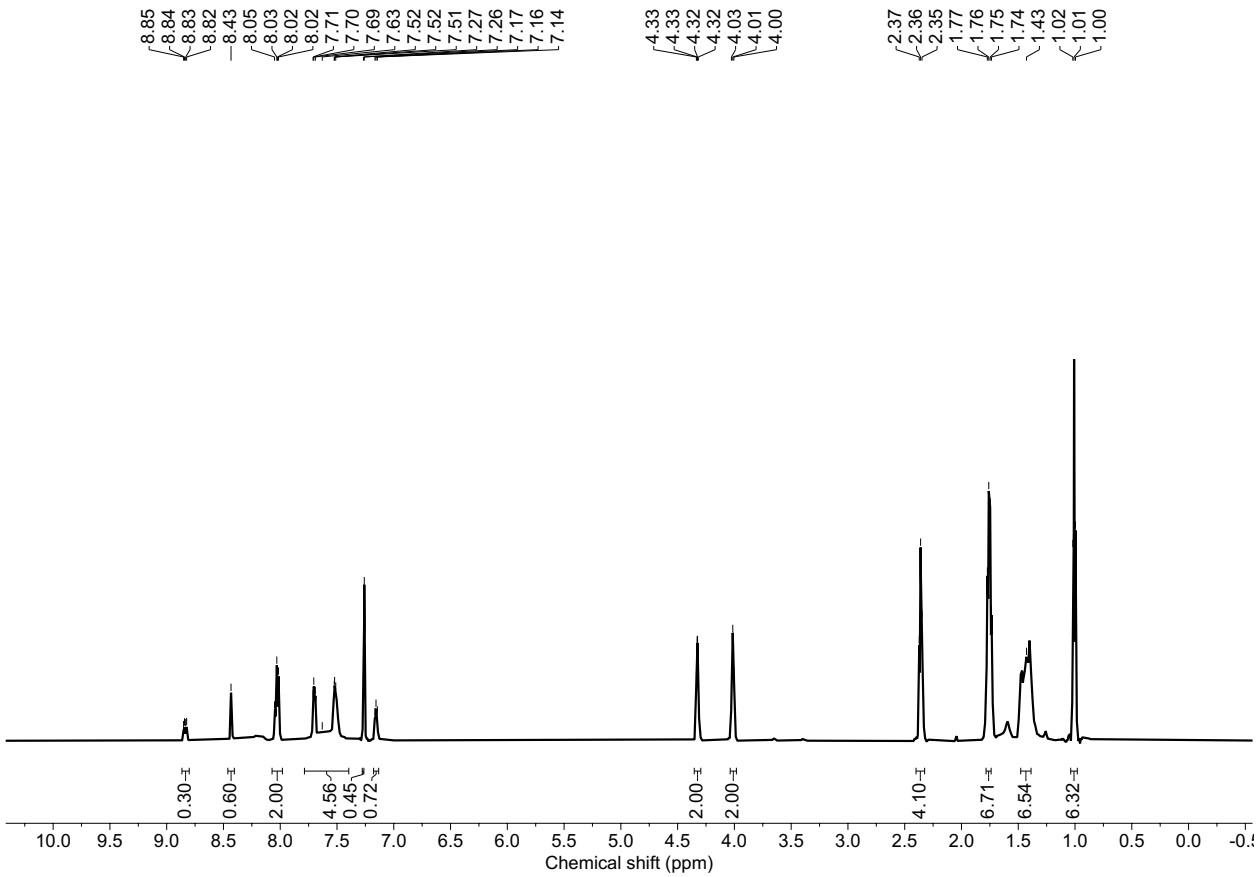

Figure S5. ^{1}H NMR spectrum of compound **2** in $CDCl_3$ (600 MHz).

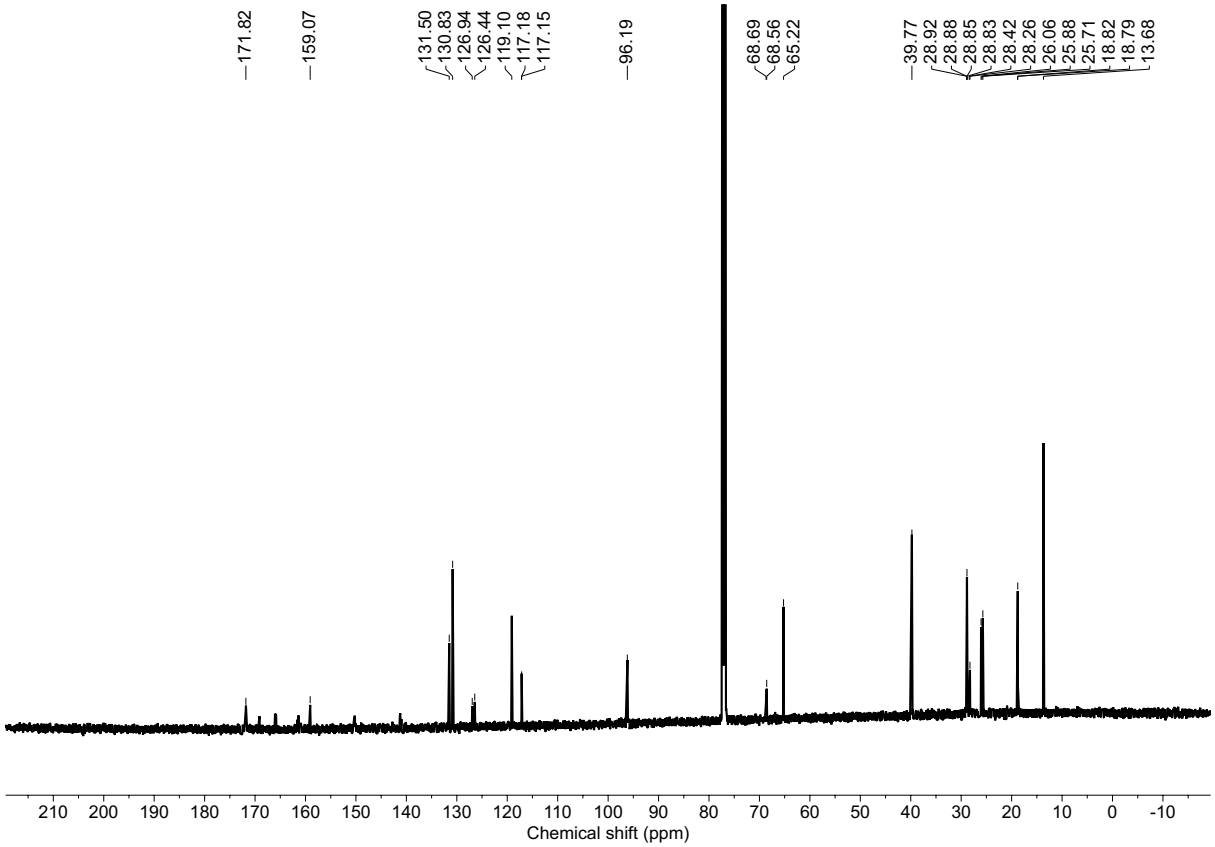

Figure S6. ^{13}C NMR spectrum of compound **2** in $CDCl_3$ (151 MHz).

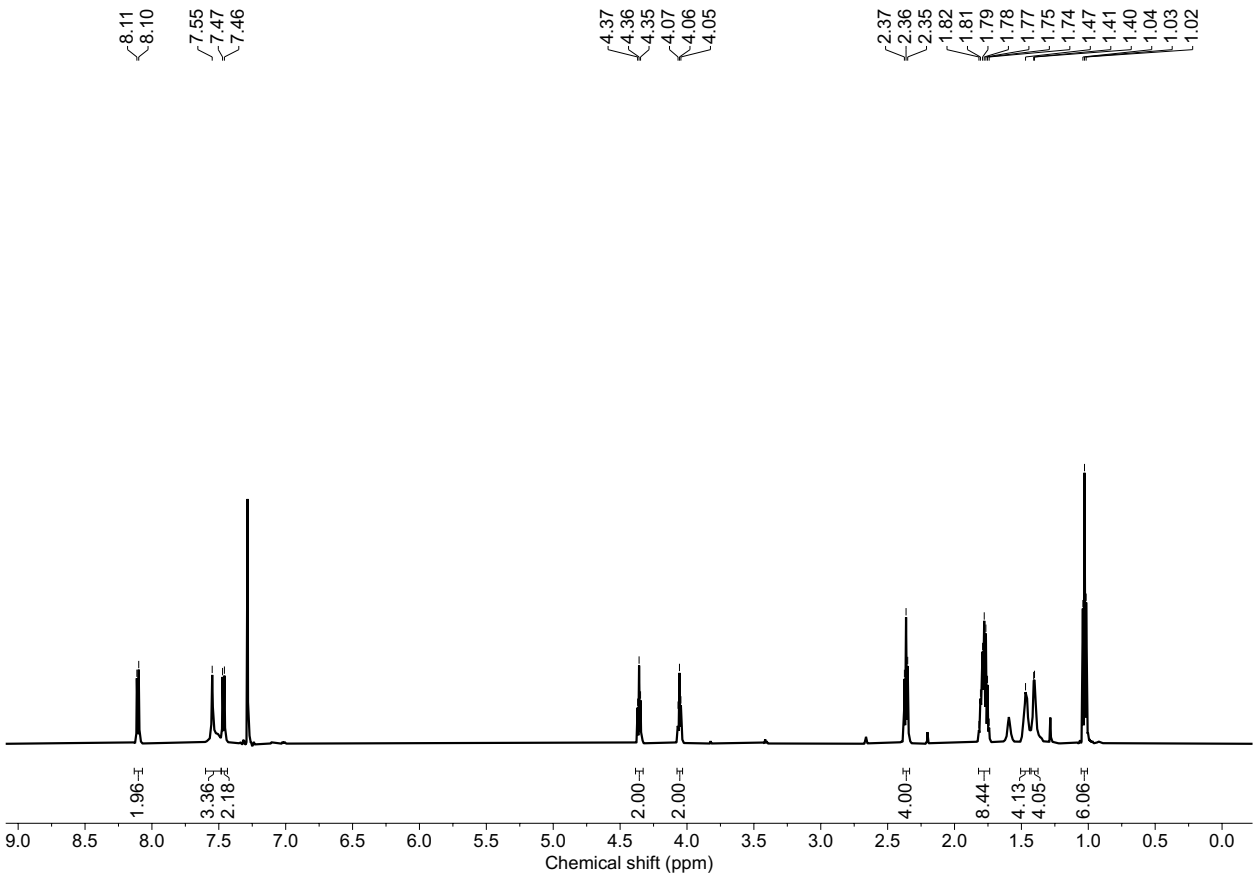

Figure S7. ^{1}H NMR spectrum of compound **3** in $CDCl_3$ (600 MHz).

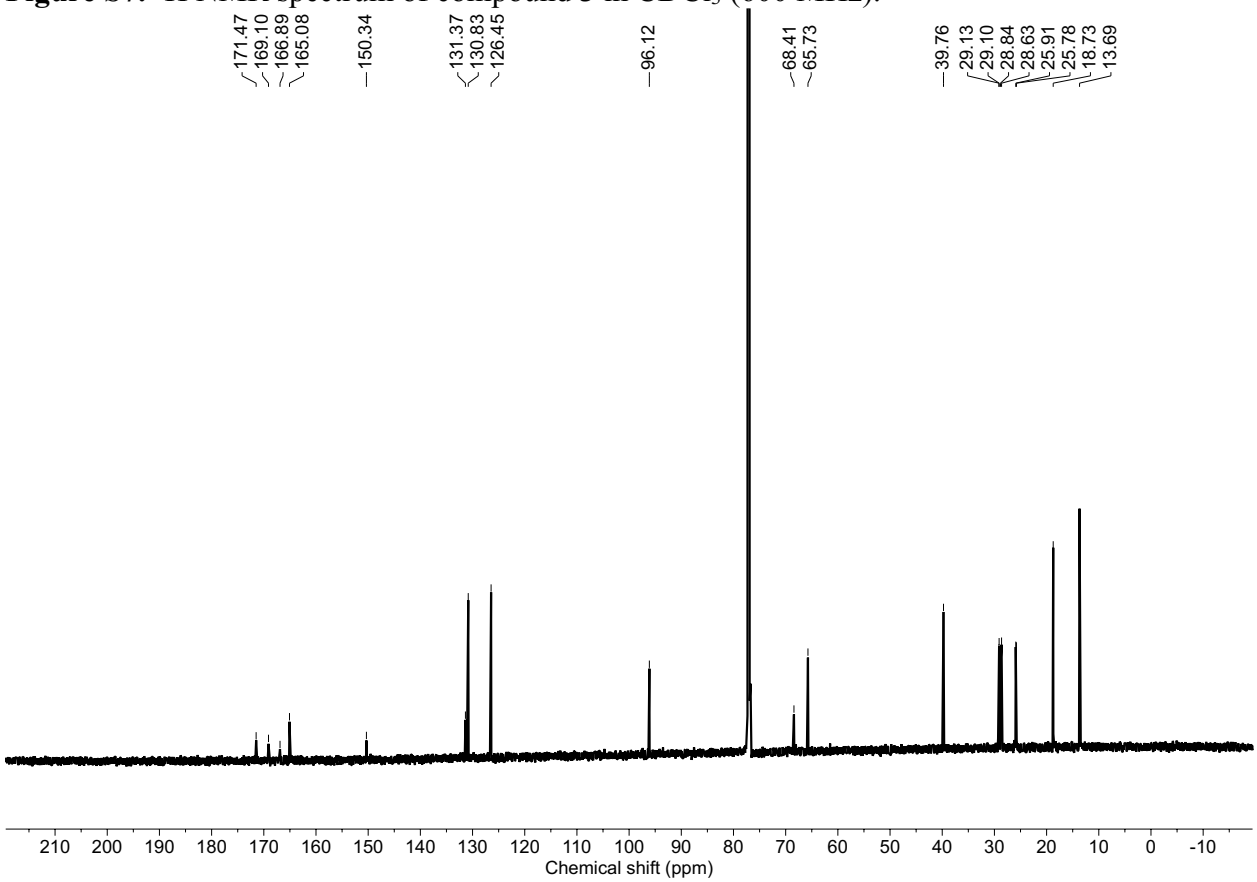

Figure S8. ^{13}C NMR spectrum of compound **3** in $CDCl_3$ (151 MHz).

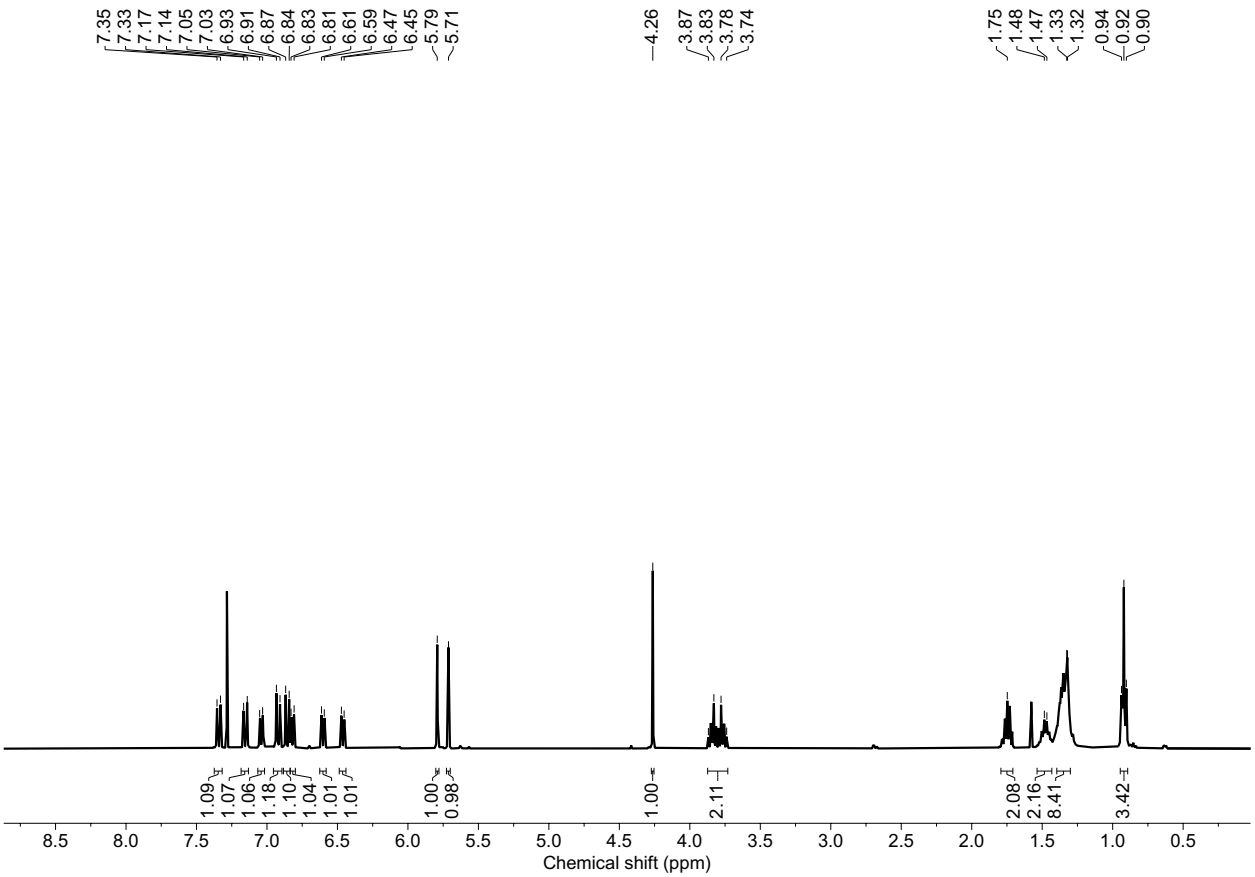

Figure S9. ^{1}H NMR spectrum of compound **4** in $CDCl_3$ (600 MHz).

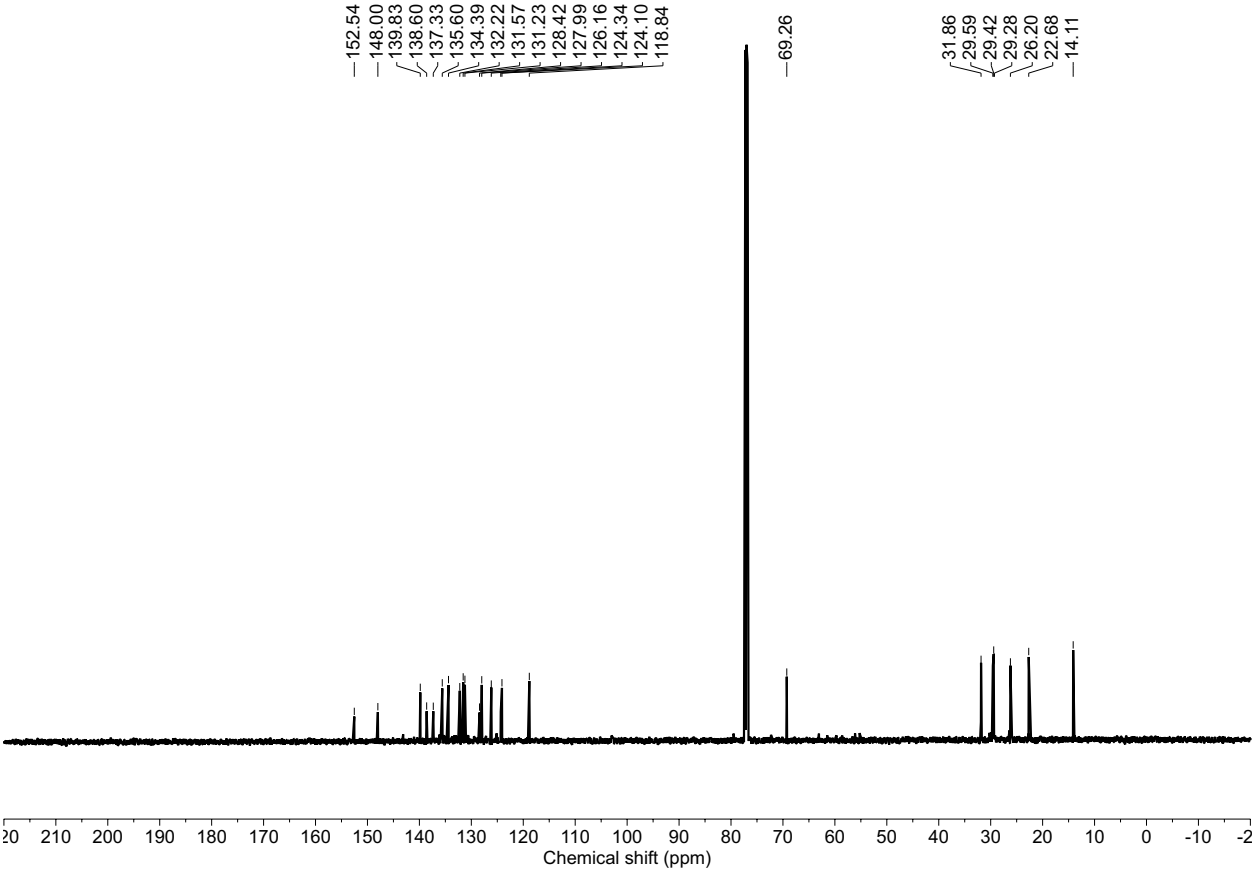

Figure S10. ^{13}C NMR spectrum of compound **4** in $CDCl_3$ (151 MHz).

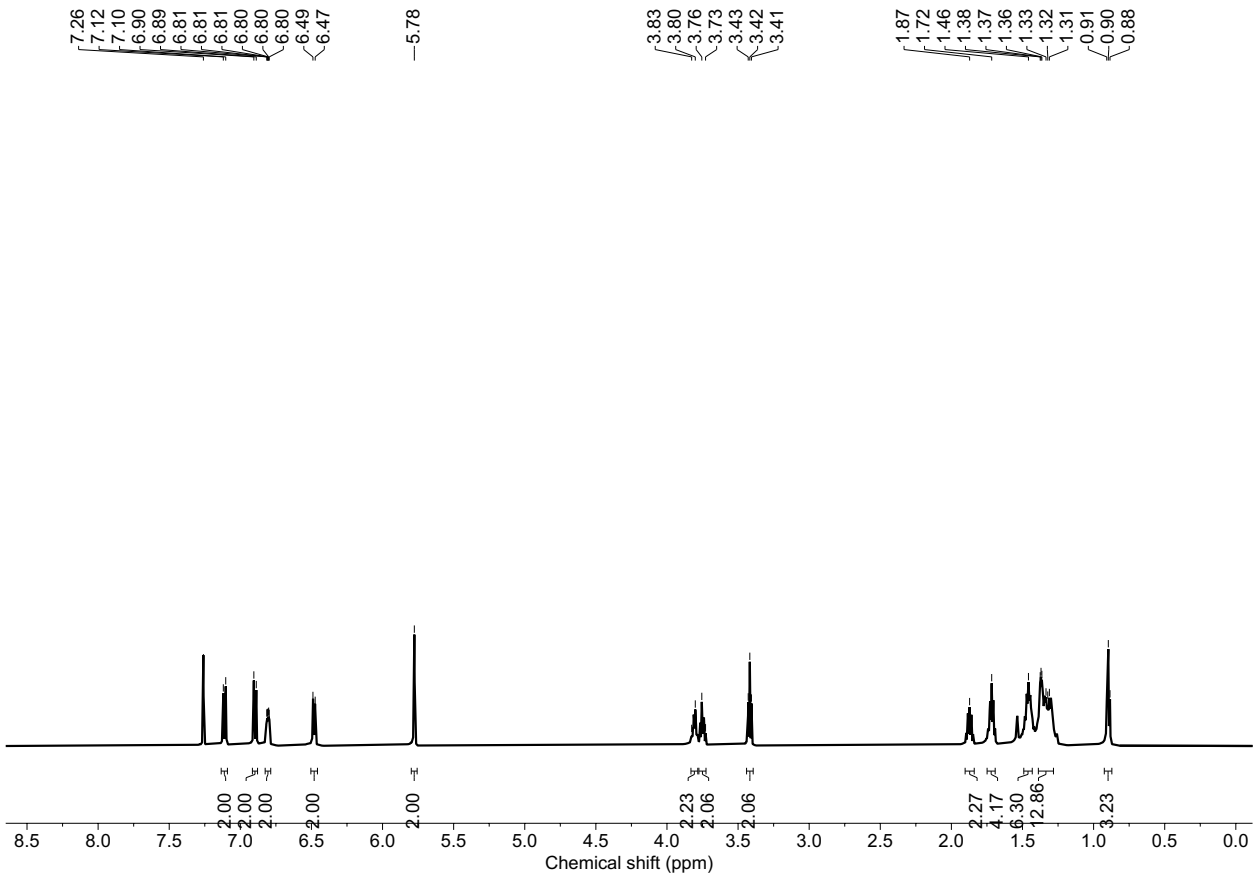

Figure S11. ^{1}H NMR spectrum of compound **5** in $CDCl_3$ (600 MHz).

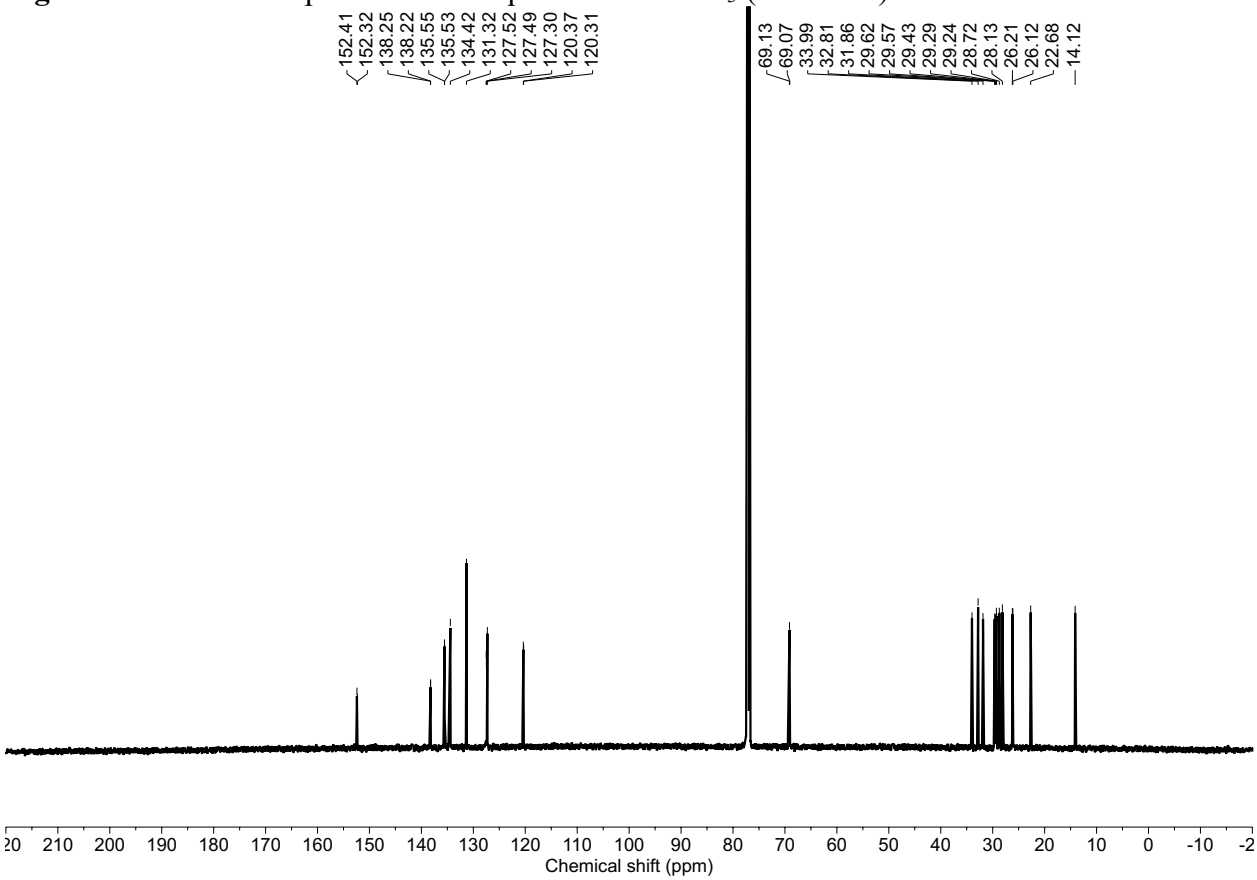

Figure S12. ^{13}C NMR spectrum of compound **5** in $CDCl_3$ (151 MHz).

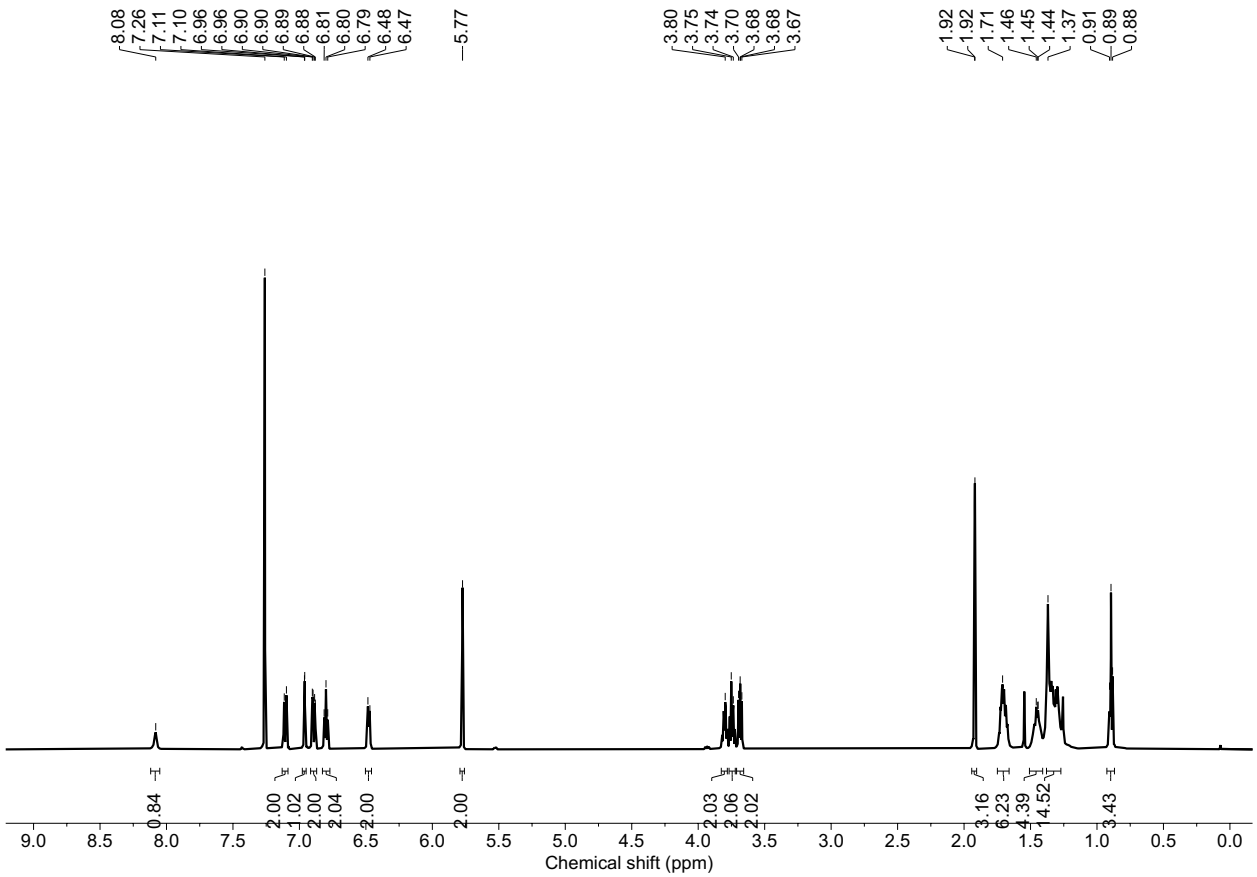

Figure S13. ^{1}H NMR spectrum of compound **6** in $CDCl_3$ (600 MHz).

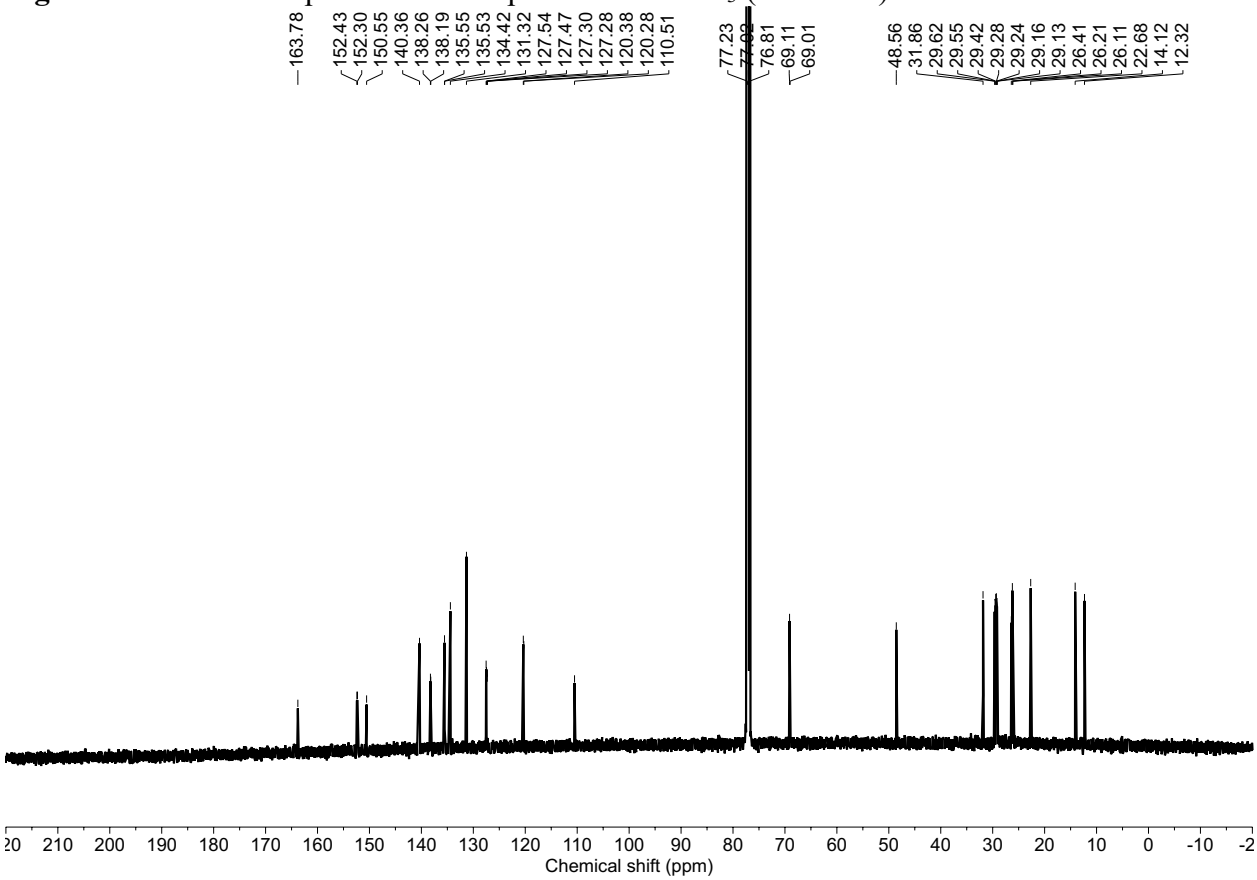

Figure S14. ^{13}C NMR spectrum of compound **6** in $CDCl_3$ (151 MHz).

Diffusion Ordered Spectroscopy (DOSY) of PPV-PIC and PPV-PIC•*N*-hexylthymine mixture

All diffusion ordered NMR spectroscopy experiments were performed on a Bruker AVIII 600 spectrometer with samples prepared in $CDCl_3$ from Cambridge Isotope Labs. Samples were kept at room temperature and stabilized at 298 K for 5 minutes in the spectrometer before data collection. For the PPV-PIC solution, the sample was prepared with a polymer concentration of 3.57 mg mL^{-1}. For the PPV-PIC•*N*-hexylthymine solution, the sample was prepared with a polymer concentration of 3.57 mg mL^{-1} and an *N*-hexylthymine concentration of 2.08 mg mL^{-1}. Prior to the DOSY experiment, ^1H NMR spectra were acquired without spinning using the convection-corrected Bruker pulse program d*stebpgp3s1d* to optimize the diffusion parameters (namely, D20 or Δ, P30 or δ/2, and the field gradient strength or GPZ6)) for the DOSY experiment. Gradient field strengths from 2% to 95% were appropriate for DOSY when D20 = 0.05 s and P30 = 1250 ms.

DOSY experiments were acquired without spinning using the convection-corrected Bruker pulse program d*stebpgp3s* as a pseudo-2-dimensional experiment with an array of 16 1-dimensional spectra spanning a linear field gradient of 2% to 95% over 16 steps. For each of these DOSY experiments, a 12 s relaxation delay (D1) was used along with a D20 (or Δ) = 0.05 s and a P30 (or δ/2) = 1250 ms.

After acquisition, spectra from individual gradient steps were manually phased and baseline corrected, and diffusion constants were obtained via processing using the topspin 3.5 T1/T2 relaxation analysis module analyzing the polymer peak in the region of 6.20 ppm – 5.50 ppm.

<u>For the PPV-PIC polymer:</u>

based on the intensity vs. field strength curve for the polymer peak in the region of 6.20 ppm – 5.50 ppm,

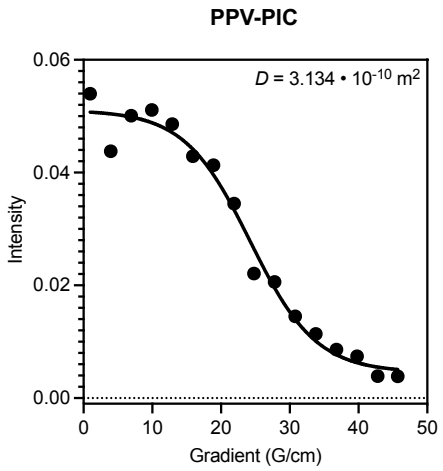

the diffusion constant is calculated to be:

$$D_{\text{PPV-PIC}} = 3.134 \bullet 10^{-10}\ \text{m}^2\ \text{s}^{-1}$$

Using the Stokes-Einstein equation (assuming a viscosity of 0.536 mPa•S), this value of $D_{\text{PPV-PIC}}$ gives a hydrodynamic radius of

$$R_{\text{PPV-PIC}} = 1.30\ \text{nm}$$

For the PPV-PIC polymer with 2.08 mg mL^{-1} of *N*-hexylthymine:

based on the intensity vs. field strength curve for the polymer peak in the region of 6.20 ppm – 5.50 ppm:

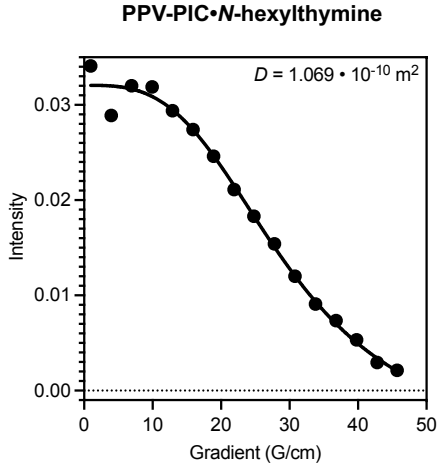

the diffusion constant is calculated to be:

$$D_{\text{PPV-PIC•Thymine}} = 1.069 \bullet 10^{-10}\ \text{m}^2\ \text{s}^{-1}$$

Using the Stokes-Einstein equation, this value of $D_{\text{PPV-PIC•Thymine}}$ gives a hydrodynamic radius of

$$R_{\text{PPV-PIC•Thymine}} = 3.81\ \text{nm}$$